PHILOSOPHICAL TRANSACTIONS OF THE ROYAL SOCIETY A MATHEMATICAL, PHYSICAL & ENGINEERING SCIENCES

Determination of the Structure of the Atmosphere between 90 and 250 km by means of Contaminant Releases at Woomera, May 1968

D. Rees

Phil. Trans. R. Soc. Lond. A 1972 **271**, 631-663
doi: 10.1098/rsta.1972.0030

DETERMINATION OF THE STRUCTURE OF THE ATMOSPHERE BETWEEN 90 AND 250 km BY MEANS OF CONTAMINANT RELEASES AT WOOMERA, MAY 1968

By D. REES

Department of Physics, University College London, U.K.

and R. G. ROPER, K. H. LLOYD and C. H. LOW

Weapons Research Establishment, Salisbury, South Australia

(*Communicated by Sir Harrie Massey, Sec.R.S. – Received* 9 *October* 1970 – *Revised* 6 *September* 1971)

[Plates 8 to 11]

CONTENTS

Two Skylark rockets were launched from Woomera rocket range, Australia (31° S) on the morning and evening of 31 May 1968. Coordinated series of measurements of neutral atmospheric wind velocity, turbulent structure, temperature and density were made during each launch between 90 and 250 km altitude, combining the experimental techniques of the two groups involved. This paper attempts to construct from the combined measurements made on these occasions a dynamic picture of the interactions of atmospheric structure, and to relate the observations to previous results obtained by ourselves and other workers.

Introduction

The basic techniques of determining upper atmospheric properties from ground-based observations of chemical clouds released from sounding rockets are well established. The two firings which are reported in this paper combine several different observational methods and experimental techniques developed by our groups, which have hitherto not been used simultaneously. The releases, from two Skylark rockets launched at Woomera (31° S) as part of the British space

Vol. 271. A. 1218. (Price £1.20; U.S. $3.35) 53 [Published 17 February 1972]

research programme, were made under twilight conditions on the morning and evening of 31 May 1968: Skylark SL 761 at 06.09 C.S.T. (20.39 U.T. 30 May) and Skylark SL 762 at 18.19 C.S.T. (08.49 U.T. 31 May). The payloads of the two rockets were similar and are listed below. For each type of release reference is made to pioneer papers describing the technique.

(i) A mass of 5 kg of trimethyl aluminium (TMA) was released as a trail between 80 and 140 km altitude, in the Earth's shadow. Chemiluminescent reactions between TMA and the ambient atmosphere give out sufficient visible radiation to enable the trail to be photographed (Rosenberg, Golomb & Allen 1963). The drift of the trail gives the atmospheric wind profile (Groves 1960). High resolution photography of the lower trail yields information on atmospheric turbulence (Blamont 1963).

(ii) Four high explosive (HEX) standard 1 lb (0.45 kg) grenades were released in succession in the trail; and charges of 5, 25 and 40 kg of high explosive were detonated on the ground, about 1 km downrange of the launcher, at such times that the shock waves produced by them reached the trail shortly after it was formed at altitudes near 100 km. The velocity of the shock waves produced by them gave the temperature of the ambient atmosphere (Rosenberg 1964).

(iii) Standard aluminium-loaded 1 lb grenades were released at intervals between 150 and 240 km altitude above the Earth's shadow. Above 190 km, multiple releases were used to maintain a nearly constant surface intensity. Aluminium monoxide, AlO, is produced, which resonantly scatters sunlight (Johnson 1965). From time-sequenced photographs of the AlO clouds, the diffusion coefficient and neutral winds may be determined (Manring, Bedinger & Knaflich 1961). Spectral observations on the band structure of the resonant radiation enable the temperature to be determined (Authier, Blamont & Carpentier 1962).

The results determined from these techniques for wind, turbulence, diffusion coefficient and temperature will be discussed in turn. Whenever observation or data reduction techniques differ from those previously reported in the literature, they will also be described. The results, and the density determined from the diffusion coefficient and temperature, are compared with the predictions of the model atmospheres.

Wind profile

With the use of standard photographic techniques, the drifts of the trail and glow clouds were determined by measuring their motion relative to the star background. The records from F 24 cameras ($f/2.9$, 200 mm focal length) at three stations were used over a period of up to 200 s after release. Motions of the cloud, and of easily identified points in the trail, were determined by direct triangulation; the smooth portions of the trail were analysed by a 'projection' computer program which made a least squares fit of the lines-of-sight from the three camera stations. The error in determined wind velocity was about 10 m s^{-1} between 100 and 200 km, and increased to 20 to 25 m s^{-1} near 90 and 240 km.

The wind profiles for the morning and evening firings are shown in figures 1 and 2 respectively. We will examine the high altitude and low altitude wind components in turn. The latter will yield information which is closely related to turbulence in the lower thermosphere; this is discussed in detail in the next section. The remarks made in this section will go no further than can be directly determined from the wind profile.

King-Hele & Scott (1967) and King-Hele (1970) have found from satellite data that at high altitudes there is a prevailing eastward mid-latitude zonal flow, with a maximum in the evening,

which increases with altitude. However, of several attempts to compute the global neutral wind pattern, Challinor (1968, 1969) alone has found a net eastward motion at high altitude and mid-latitude. He has calculated the global wind patterns at 250 km assuming that electrodynamic drag between ions and neutrals is dominant in the daytime, but at night, the pressure gradients take control.

Our own observations reported here, which show winds predominantly southward at 100 m s^{-1}

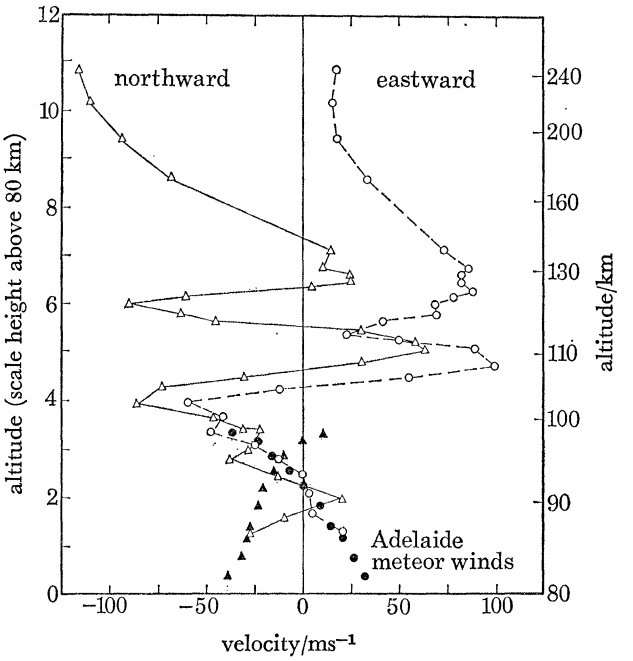

FIGURE 1. Morning wind profile.

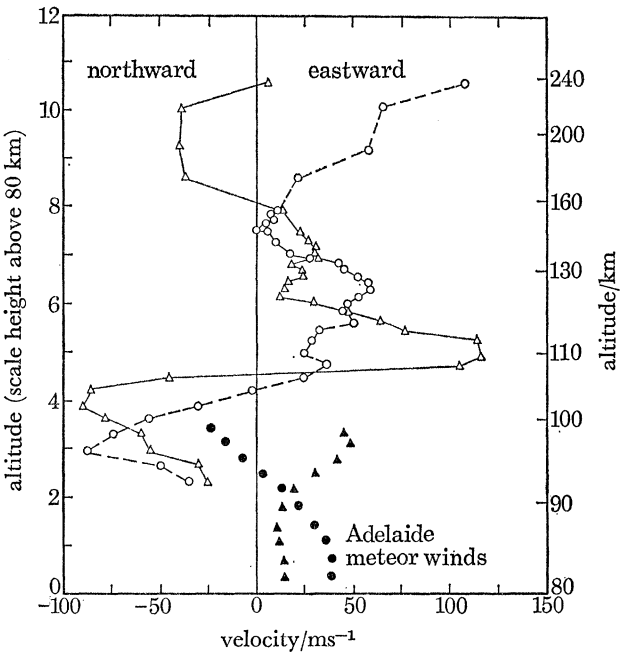

FIGURE 2. Evening wind profile.

PHILOSOPHICAL TRANSACTIONS OF THE ROYAL SOCIETY A MATHEMATICAL, PHYSICAL & ENGINEERING SCIENCES

in the morning and east–south–east at 75 m s^{-1} in the evening, demonstrate the evening eastward wind as with King-Hele & Scott's results, and also show the presence of strong meridional winds at the 200 km level.

Recently we have examined a greater amount of experimental data, of both thermospheric neutral winds (Lloyd *et al.* 1972) and neutral temperature (Rees 1971) in an attempt to resolve the discrepancies between computed and observed winds in the thermosphere. All the computed models derive from Harris & Priester (1962) or Jacchia (1965) global temperature and density models. Rees (1972) has queried the latitudinal variation of these two models and proposed that the global minima of temperature and pressure occur near the poles and not at the anti-solar point during geomagnetically quiet periods.

We have proposed that the eastward evening wind and seasonal variations we have observed in the meridional wind component, averaging 60 m s^{-1} from summer to winter pole at both morning and evening twilight at mid-latitude, arise as a pseudo-geostrophic wind due to the global pressure system (with minima near the poles), and due to inter-hemispheric asymmetry caused by low air density above the winter pole (150 to 190 km altitude) and the seasonal migration in latitude of the low latitude diurnal temperature and density bulge.

Due and reasonable allowance being made for ion drag in the day period, this simple model appears to account for the major features of mid-latitude thermospheric neutral winds at 200 to 300 km during geomagnetically quiet periods.

M. A. MacLeod (1965, private communication) suggested the use of a scale height unit (ζ) defined by

$$\zeta = \int_{80}^{h} \mathrm{d}h/H,$$

where H is the pressure scale height as an empirical dimensionless unit to describe the vertical variations of the neutral wind profile above a base level of 80 km.

There is no generally accepted reason why wind profiles expressed in these units are frequently regularly periodic; however, it is a very convenient method of determining the regular and random components of a particular neutral wind profile. Also, plotting the altitude on a scale in which the wavelength is nearly invariant, enables an estimate of the wavelength to be determined by auto-correlation techniques. It is seen immediately, however, from figures 1 and 2 that, even on this altitude-foreshortened scale, the wavelength increases with altitude, and at the highest altitudes seems to have become a steady flow. Figure 3 shows the auto-correlation and cross-correlation functions for the winds determined from the trail on the evening firing, SL 762. The main feature is that all the functions go to zero at about 0.8 scale heights. This means that the dominant wavelength in these altitudes is a little over three scale heights; i.e. a wavelength of 20, 37 and 70 km at 100, 120 and 150 km respectively. This agrees very well with the mean wavelength of 3.0 scale heights which Rosenberg & Justus (1966) observed from their analysis of 15 trails.

The cross-correlation function for the firings also shows that the north–south wind component is in advance of the east–west component by about a quarter wavelength, i.e. the profile describes a circular helix progressing counterclockwise with increasing altitude. Rosenberg (1968*a*), in an analysis of 70 wind profiles in the Northern Hemisphere, found the phase progression to be clockwise. This dependence of the rotation on the hemisphere is just what is expected for tidal winds, and so it is reasonable to associate the rotation of the wind vector with altitude (i.e. circular polarization) with the tidal component of the wind. Possibly the dominant tidal mode is the

diurnal (1, 1) mode (Hines 1968) since its wavelength at 100 km, which is 24 km (Lindzen 1966), is close to the observed wavelength.

In order to make an unambiguous distinction between tidal waves and internal gravity waves it is necessary to have a series of trails separated in time by less than the shortest wave period – and this we do not have. However, we do have some knowledge of the prevailing, diurnal and semi-diurnal wind components between 80 and 100 km, as measured by the University of Adelaide radio meteor wind equipment (Adelaide is 450 km southeast of Woomera). The meteor wind profiles for the appropriate times, constructed from the means of the measured May and June 1968 prevailing, diurnal and semidiurnal wind components only, are also plotted in figures 1 and 2. These results have been kindly communicated to us by Elford & Doyle (1972). A profile containing only mean prevailing, diurnal and semidiurnal components adequately describes our measured morning wind profile to 100 km, whereas, in the evening, significant departure from these means is evident. The better agreement between the Adelaide and Woomera wind profiles in the morning than in the evening, confirms the deduction made in the next section that the contribution of smaller scale motions, such as gravity waves and turbulence, is less in the morning. Furthermore, the zonal winds are in better agreement than the meridional, as we would expect. In later trials (Lloyd *et al.* 1972), meteor winds have been obtained at the time of firing, enabling an estimate of the Rossby global waves to be obtained from the phase shift in the meridional wind between Woomera and Adelaide.

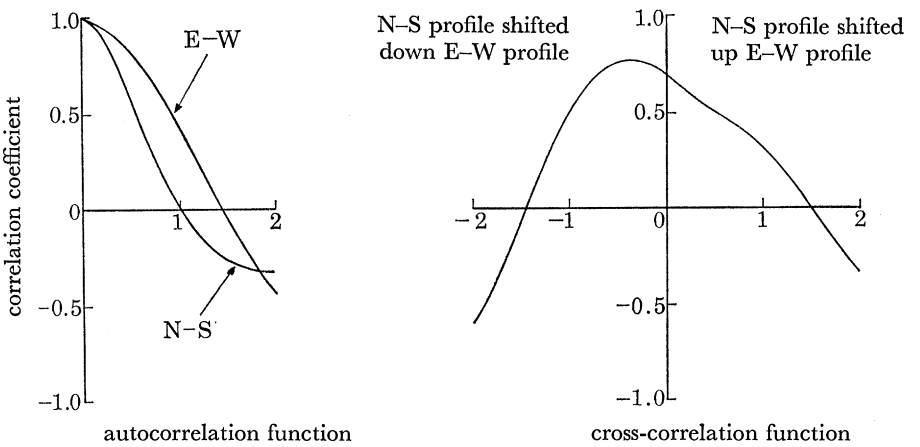

FIGURE 3. Correlation functions for evening wind profile. The abscissae are altitude shift (scale heights, ζ). These curves were derived from the wind profile of figure 2, over the altitude interval 92 to 130 km.

TURBULENCE

Rocket-borne mass spectrometer measurements of atmospheric constituents and observations of vapour trails in the upper atmosphere have shown that the atmosphere is thoroughly mixed to a height of 105 ± 5 km. This height, known as the turbopause, is usually clearly marked on each vapour trail – below the turbopause the trail is 'obviously turbulent'. That the observed structure is indeed due to ambient atmospheric turbulence has been discussed by Blamont (1963); that the structure is not caused by either the ejected material or its method of release is demonstrated by the fact that the analysis of observations of different materials (e.g. sodium and trimethyl aluminium) ejected from rockets, and of meteor trails (observed both optically and using radio

techniques), and the theoretically deduced eddy diffusivities required for both the maintenance of the energy budget of the mesosphere and lower thermosphere and the observed ratio of atmospheric constituents above the turbopause, all lead to consistent values of the ambient turbulence intensity.

Above the turbopause the trail appears laminar and diffuses with cylindrical symmetry. However, it is observed that the trail below the turbopause does not become 'obviously' turbulent until some time after release; when it does show signs of breaking up the dehiscence occurs very rapidly. Some excellent time sequence exposures of both the morning and evening trails were obtained with the Smithsonian Institution's satellite tracking Baker Nunn camera, located at Island Lagoon, 160 km from the Skylark launcher. The Baker Nunn is an $f/1$, 50 cm focal length camera, with a field of view up to $25° \times 5°$. A $5° \times 5°$ format was used for these trials. Since the camera is located behind the launcher, the full length of each trail fell within the field of view and was recorded as detailed in table 1.

TABLE 1. BAKER NUNN EXPOSURE SEQUENCES

	seconds after release		frame rate	exposure
firing	from	to	s^{-1}	s
SL761	0	17	1	0.2
	28	103	0.5	0.4
	camera retrained on high altitude glows			
SL762	0	12	1	0.2
	24	58	0.5	0.4
	66	114	0.25	0.8
	camera retrained on high altitude glows			

Neither trail was sunlit, and the radiation observed was the continuum emitted by the trimethyl aluminium reacting chemiluminescently with the ambient (Rosenberg *et al.* 1963). The release of TMA is much less violent than that of sodium, and we may assume that the behaviour of the trail at times greater than 10 s after release, represents motions of the ambient atmosphere (Blamont & Barat 1968).

Isodensitrace scans of part of the trail from each firing are presented in figures 4 and 5, plates 8 and 9, to illustrate the delay in the onset of turbulence. A further sequence of that portion of the evening trail just above the turbopause is also given in figure 5 to show that, while there is no evidence whatsoever of trail break-up (i.e. the trail remains laminar), its diameter increases by diffusion at a rate considerably greater than could be produced by molecular diffusion alone. Diffusion greater than molecular is evident on both trails up to heights of about 120 to 130 km (see section on diffusion).

Blamont (1963) has argued that a vapour trail will not become 'obviously turbulent' until sufficient time has elapsed for the trail to reach a dimension comparable with that of the smallest eddy of the turbulence spectrum. He concentrated on the scale size of the smallest eddies, producing evidence from high resolution photography of a sodium trail that the smallest eddy was of the order of 50 m.

We find that the trail reaches an observable diameter far in excess of 50 m before it shows any sign of turbulent motion, even though after trail break-up occurs elements as small as 50 m in diameter are observed. Note that the trail radius of table 2 is the 'effective radius', defined by Lloyd & Sheppard (1966) as the radius at which the cloud radiance falls to 1/e of its central

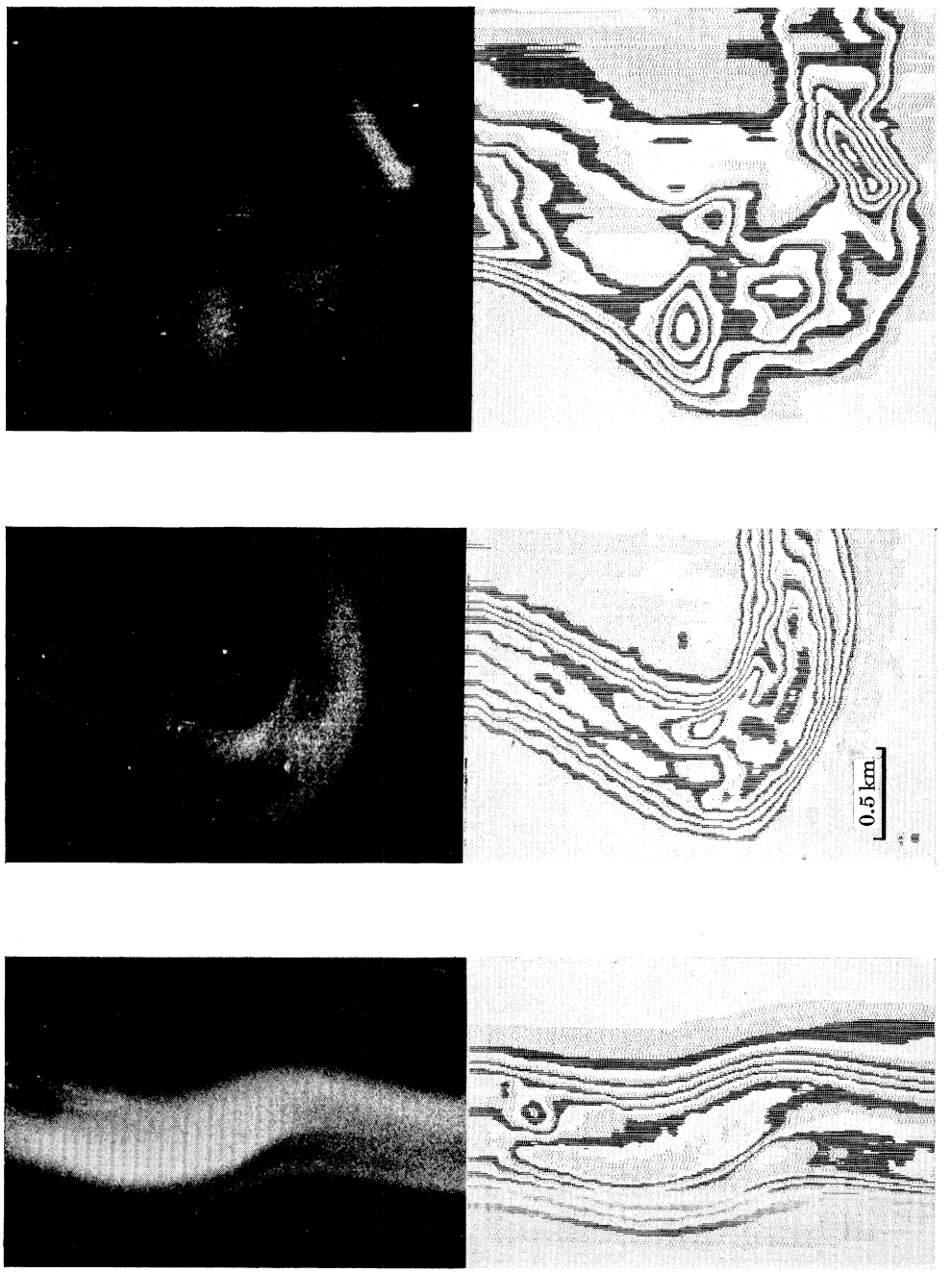

FIGURE 4. Montage of portion of the morning trail. The kink is at an altitude of 102.7 km. Note that the trail is laminar at +30 s, and that the trail diameter at this time is greater than the scale of the eddies at +50 s.

(*Facing p.* 636)

PHILOSOPHICAL TRANSACTIONS OF THE ROYAL SOCIETY A MATHEMATICAL, PHYSICAL & ENGINEERING SCIENCES

PHILOSOPHICAL TRANSACTIONS OF THE ROYAL SOCIETY A MATHEMATICAL, PHYSICAL & ENGINEERING SCIENCES

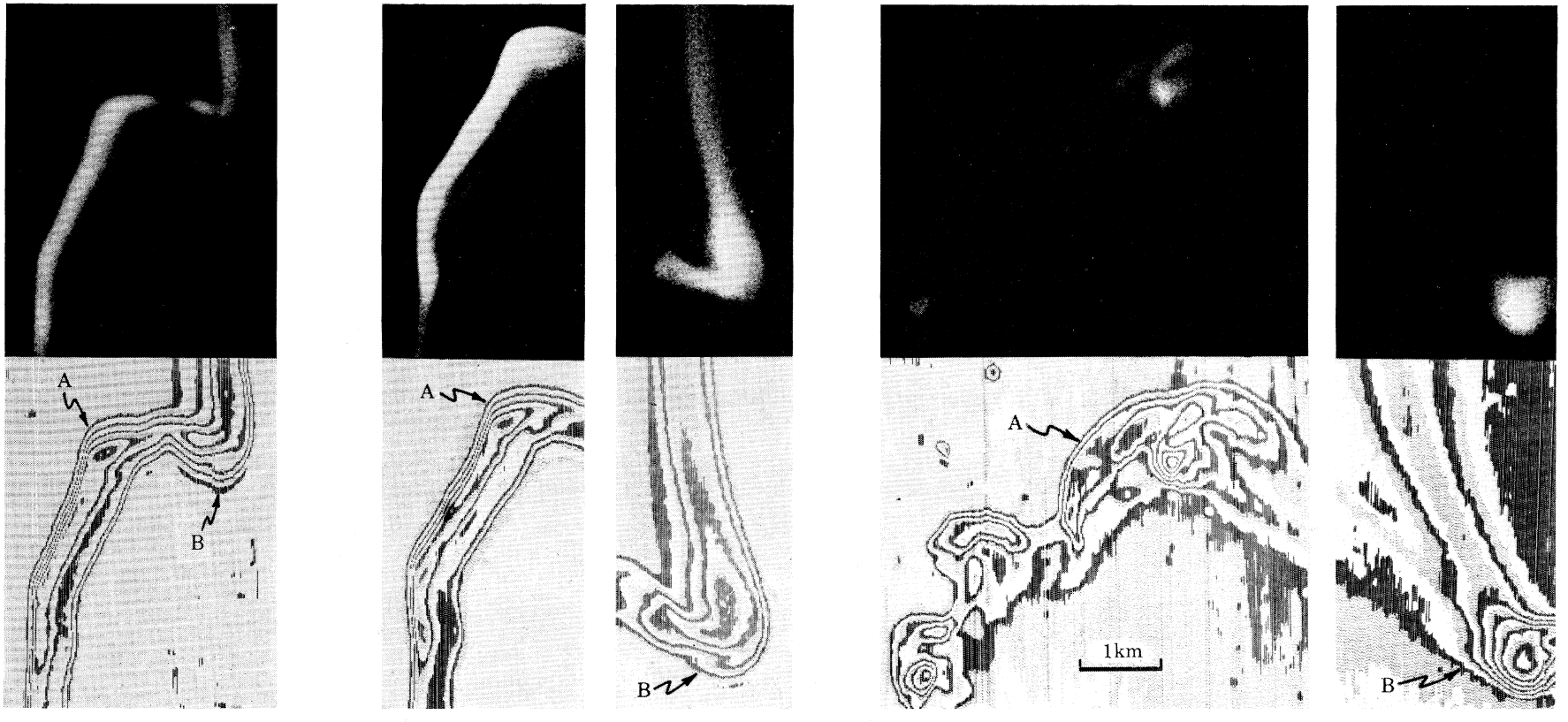

$t = +9$ $+7$ $+23$ $+21$ $+61$ $+59$ s

FIGURE 5. Montage of portions of the evening trail. Points A and B are at 106 and 108 km altitude respectively. Note the transition from laminar to turbulent structure at A between +23 and +61 s. This has not occurred at B.

PHILOSOPHICAL TRANSACTIONS OF THE ROYAL SOCIETY A MATHEMATICAL, PHYSICAL & ENGINEERING SCIENCES

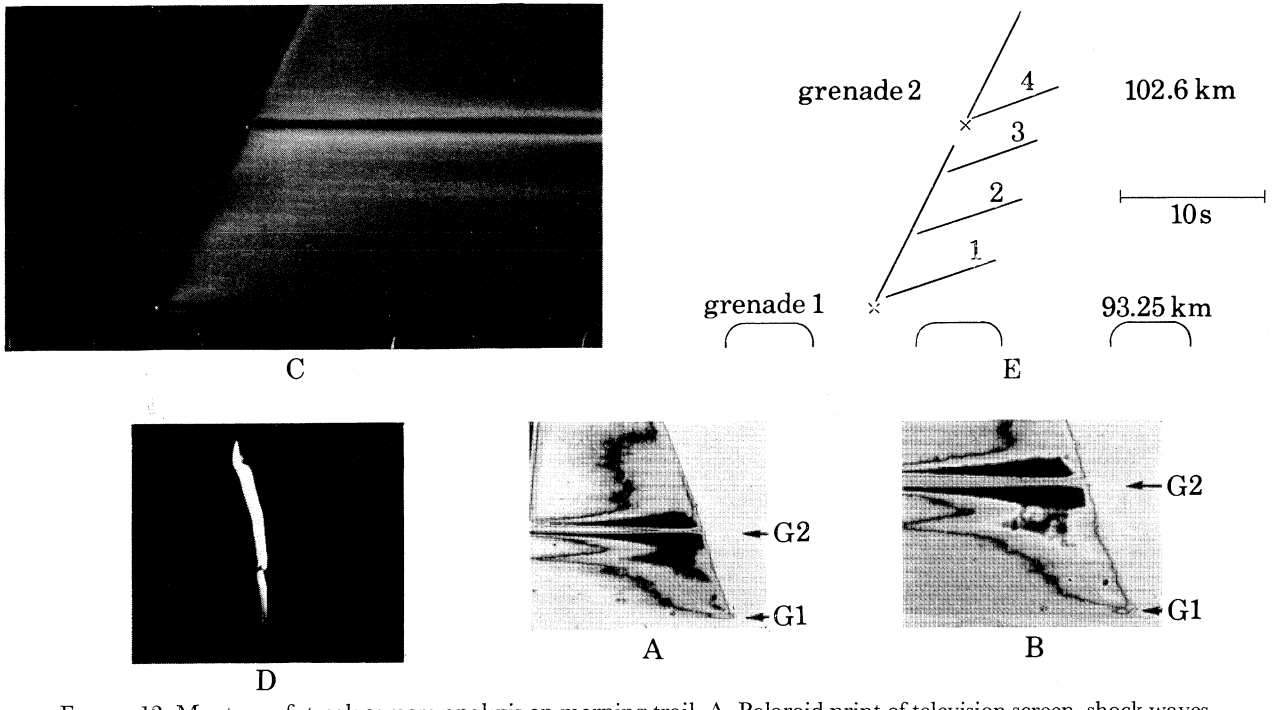

FIGURE 12. Montage of streak camera analysis on morning trail. A, Polaroid print of television screen, shock waves as light features. B, Polaroid print of television screen, shock waves as dark features. C, Print of streak camera photograph. D, Baker Nunn photograph at 78 s after launch. E, Identification of measured features: 1, upward shock wave envelope of G 1; 2, ground shock wave 3 (40 kg); 3, ground shock wave 2 (20 kg); 4, upward shock wave envelope of G 2.

PHILOSOPHICAL TRANSACTIONS OF THE ROYAL SOCIETY A MATHEMATICAL, PHYSICAL & ENGINEERING SCIENCES

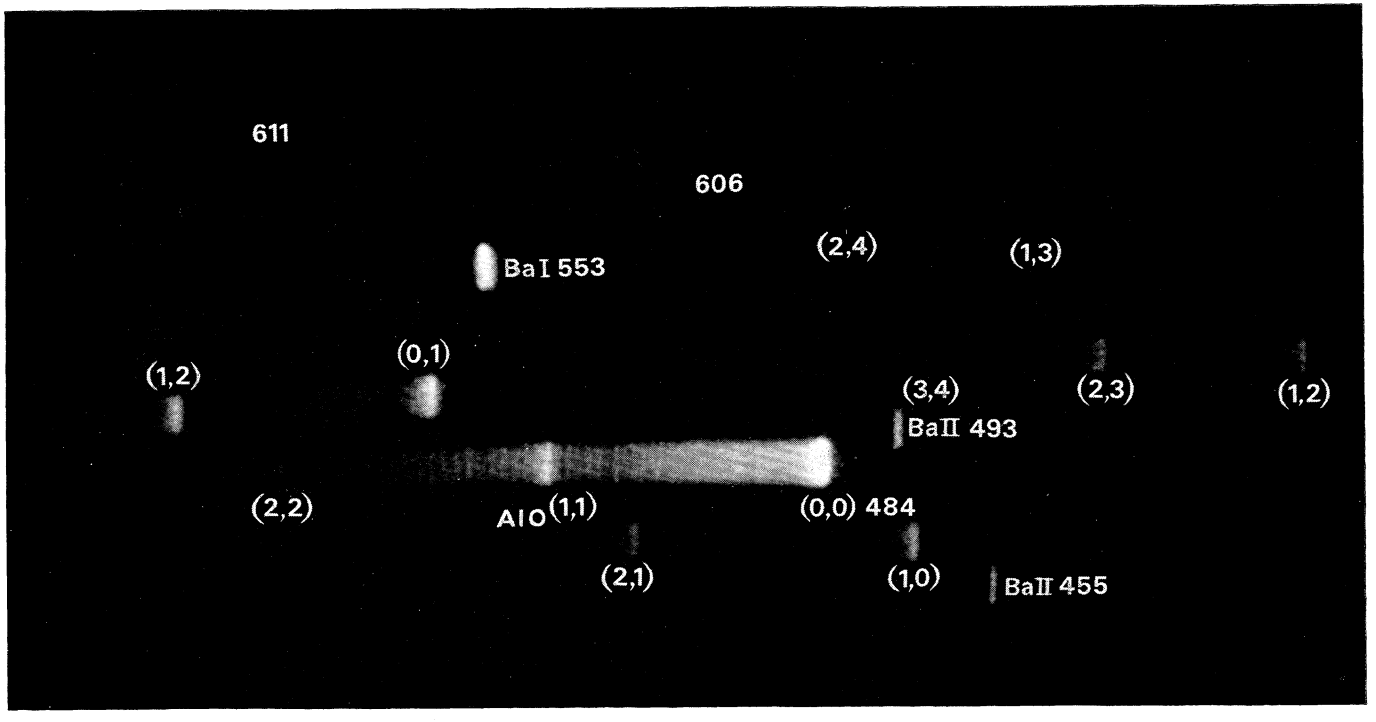

FIGURE 14. Echelle plate from the glow cloud at 187 km on the evening firing. The features observed from all the glow clouds on trials SL761 and SL762 are listed.

barium lines		AlO					
Ba I	Ba II	order	λ/nm	band	order	λ/nm	band
553.5	455.4	46	536	(1, 3)	48	508	(0, 1)
582.6	493.4	46	538	(2, 4)	48	510	(1, 2)
597.7	614.2	46	539	(3, 5)	50	484	(0, 0)
599.7	649.2	47	510	(1, 2)	50	487	(1, 1)
606.3		47	512	(2, 3)	50	489	(2, 2)
611.0		47	514	(3, 4)	52	465	(1, 0)
634.2		47	516	(4, 5)	52	467	(2, 1)
649.9							
652.7							
667.5							
669.3							
706.0							

maximum. The 'observable diameter' is considerably greater, as can be seen from the scales on the isodensitrace montages of figures 4 and 5. Our observations suggest that Blamont's (1963) criterion for the trail break-up is invalid. We have evidence that the important factor is the time after deposition, rather than the length scale of the motion involved. The times taken between the deposition of the trail, and its eventual breakdown under the action of turbulent eddies, for several identifiable features on each trail, are presented in table 2.

TABLE 2. TIME LAG IN ONSET OF TURBULENCE

	altitude / km	t^* / s	Δt / s	trail radius r_e^*/m at t^*
SL761	86	12	3	30
	90	20	4	40
	97.6	22	4	80
	99.5	25	4	90
	101	29	4	100
	102.7	38	4	110
	103.5	55	4	120
SL762	94	9	3	60
	96	13	3	60
	99	14	3	100
	104.2	22	4	110
	105	33	4	140
	106	49	6	150

Δt is a measure of the error in t^*, and is the time taken for the trail to change from 'obviously laminar' to 'obviously turbulent'.

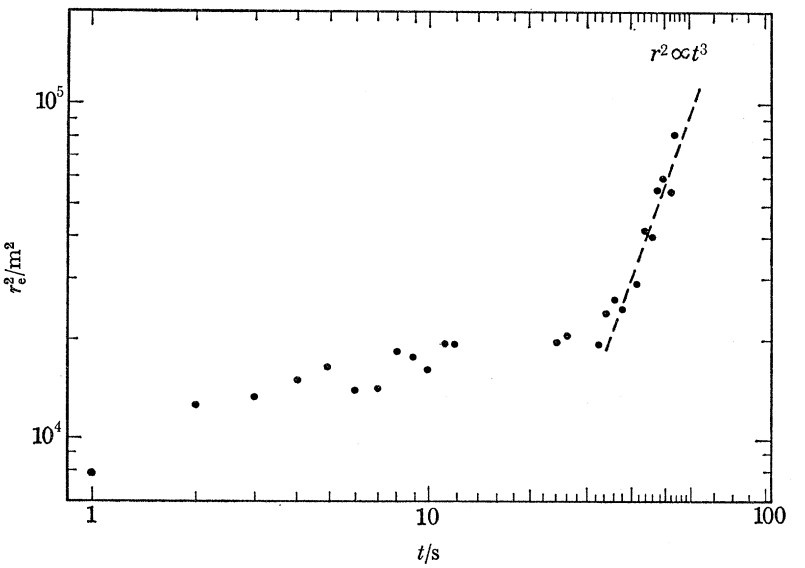

FIGURE 6. Variation of radius with time after release at 105 km.

That the breakdown from 'obviously laminar' to 'obviously turbulent' represents a dramatic change, easily recognized by visual inspection of the film, is shown in figure 6 in which the square of the effective radius is plotted against time after release for the evening trail at 105 km. We would venture to say that this is the only phase of contaminant release growth that does not require extremely careful measurement to reveal the true behaviour.

The growth in the first few seconds after release is an order of magnitude faster than the

subsequent growth up to the time of trail breakdown, and is therefore regarded as representing the release phase in which the energetics are definitely non-ambient. The growth between 8 and 32 s after release could be molecular diffusion of a cloud with an initial radius of approximately 130 m, i.e. the release phase produces a cloud with, effectively, this radius at zero time. However, we can only say that the growth during this period could be molecular – the 15 % error in the determination of the effective radius from each film frame, and the fact that the trail cross-section is only approximately Gaussian, precludes a measurement of diffusion coefficient to better than a factor of 3. The onset of turbulence occurs 33 s after release, and then proceeds as

$$r_e^2 \propto t^3,$$

until, at 54 s, the trail becomes too irregular for an estimate of radius based on a Gaussian distribution to be meaningful.

Before any theoretical prediction of appropriate time or length scales can be attempted, the nature of the turbulent flow field must be defined. Blamont & Barat (1967*a*, 1968) have divided the region below the turbopause into two height ranges, with 100 km as the dividing altitude. They consider the region above 100 km to be a domain of pseudoinertiality and high dissipation, and below 100 km to be a region of weak, anisotropic turbulence governed principally by buoyancy forces. In doing so they lean heavily on the work of Bolgiano (1959, 1962), and claim that his theory applies to an anomalous phase in the observed growth of their trails, which occurs, on average, some 150 s after release (Blamont & Barat 1968, figure 1). Neither of the trails reported here showed such behaviour; the transition from laminar to dehiscent appearance occupies at most some 6 s, and occurs less than 60 s after release (see table 2). We cannot comment on late time behaviour, since neither trail was photographed by the Baker Nunn camera for 150 s (see table 1); however, some 35 mm camera photographs suggested that trail break-up occurred rapidly, and at about 180 s at 112 km.

While acknowledging that buoyancy does play a considerable role in the motions observed at these altitudes, we believe we have sufficient evidence for a dissipation mechanism which, at all levels, involves a predominantly horizontal cascade of energy through highly anisotropic eddies. To justify this approach, we rely on the work of Lumley (1964), who emphasizes that the effect of buoyancy on a turbulence spectrum depends on the rate of work done by the specific buoyancy force, rather than the intensity of that force. The evidence for horizontal correlation is taken from Roper (1966*a*), who shows, from meteor trail results, that the velocity difference between two points separated by some 500 m up to 3.5 km follows

$$\overline{\Delta v^2(r)} \propto r^{\frac{2}{3}};$$

from Justus (1967*a*), who finds that horizontal spatial correlation extends up to 7.5 km horizontal separation; and to a lesser degree from Justus & Roper (1968), who found, from simultaneous observations of two vapour trails separated by a large distance, that horizontal correlation extended up to 100 km. Further support for horizontal correlation at these much larger scales comes from the treatment by Roper & Elford (1963) of Greenhow & Neufeld's (1959) time correlation function for random meteor wind motions; this treatment indicates that horizontal scales with characteristic time constants of up to 100 min (length scale 150 km) are correlated.

We visualize the atmosphere at these heights as being stratified by buoyancy forces into layers approximately 1 km thick, with vertical motion allowed within the layers, so that scales of dimension less than 1 km are probably isotropic; and with the vertical profile of the horizontal wind

correlated by the shearing stress between the layers. The strata thickness is somewhat arbitrary, and is chosen as 1 km simply because observations by others (for example Blamont & de Jager (1961) and Blamont (1963)) indicate that motions with scales less than 1 km are isotropic. Measurements of grenade glow clouds by Rofe (1961) and Rees (1969) and of vapour trail globules by Justus (1966), show from their vertical movements that they are confined to layers varying in thickness from 500 m at 90 km to 2 km at 110 km. Our model does not preclude the alternation of laminar and turbulent regions observed by Blamont & Barat (1967*b*) – non-turbulent layers could exist between turbulent layers if the wind velocities and the shearing stresses were not large or if there were multiple inversions in the temperature profile.

Because the smaller eddies have shorter time constants, their effect on the dispersion of the trail will be observed first. Batchelor (1953, p. 115), after Kolmogoroff (1941), defines the basic length parameter of the viscous dissipation (small scale) region as

$$\eta = (\nu^3/\epsilon)^{\frac{1}{4}},$$

where ν is the kinematic viscosity, ϵ is the rate of dissipation of turbulent energy, and η is in metre/radian. Expressed as a wavelength (metre/cycle)

$$\eta = 2\pi(\nu^3/\epsilon)^{\frac{1}{4}}. \tag{1}$$

It is this parameter which Blamont (1963) associates with trail breakup.

Batchelor (p. 150) also defines this unit length scale in terms of a characteristic time constant t^* such that

$$\eta = (\nu t^*)^{\frac{1}{2}}.$$

When η is again expressed in metre/cycle, this equation becomes

$$\eta/2\pi = (\nu t^*)^{\frac{1}{2}}. \tag{2}$$

Combining equations (1) and (2) yields

$$t^* = (\nu/\epsilon)^{\frac{1}{2}}. \tag{3}$$

We shall show that it is this parameter which is associated with trail break-up.

Roper (1966*b*), using wind shear results published by Kochanski (1964), has calculated the variation with height, h km, of the rate of dissipation of turbulent energy ϵ. The kinematic viscosity ν may be determined from the viscosity, μ, and density, ρ, of the *U.S. Standard Atmosphere Supplements* (1966). The function

$$\nu(\mathrm{m^2/s}) = \exp[0.17(h-80.0)],$$

with h in kilometres, was found to fit the data at the tabulated altitudes, and was used to compute ν at 1 km height intervals. These values of ϵ and ν are coupled to produce what can be regarded as average height dependent characteristic length scales η_R (from equation (2)) and time scales t^*_R(from equation (3)). These have been tabulated in table 3.

A more direct measure of the average turbulent dissipation rate profile has been made by Justus (1967*b*), whose results are presented in table 4, together with the appropriate time and length scales t^*_J and η_J. The variation of t^*_R and t^*_J with height are also plotted in figure 7, and the variation of η_R and η_J with height are plotted in figure 8.

The similarity in form, and the order of agreement, between the predicted 'average' trail time constants t^*_R and t^*_J and the measured values for each of the two releases is surprisingly good when one considers the approximations involved in: (*a*) the model atmosphere viscosity, which is

TABLE 3. VARIATION WITH ALTITUDE OF THE CONSTANTS OF THE KOLMOGOROFF MICROSCALE (AFTER ROPER 1966*a*)

altitude / km	ϵ_R / W kg^{-1}	t_R^* / s	η_R / m
80	0.01	10.0	19.0
81	0.011	10.4	22.0
82	0.0118	10.9	24.6
83	0.0128	11.4	27.4
84	0.0139	11.9	30.5
85	0.015	12.5	33.9
86	0.016	13.2	37.9
87	0.017	13.9	42.4
88	0.0185	14.5	47.2
89	0.0198	15.3	52.8
90	0.021	16.1	59.0
91	0.023	16.8	65.6
92	0.025	17.5	73.0
93	0.027	18.4	81.3
94	0.030	19.0	90.0
95	0.033	19.7	100
96	0.038	20.0	109
97	0.042	20.7	121
98	0.049	20.9	132
99	0.057	21.0	145
100	0.066	21.3	159
101	0.080	21.0	172
102	0.098	20.7	186
103	0.125	19.8	195
104	0.168	18.8	209
105	0.186	19.4	232
106	0.20	20.4	259
107	0.15	25.6	316
108	0.085	37.0	413
109	0.033	64.7	595
110	0.01	128	911

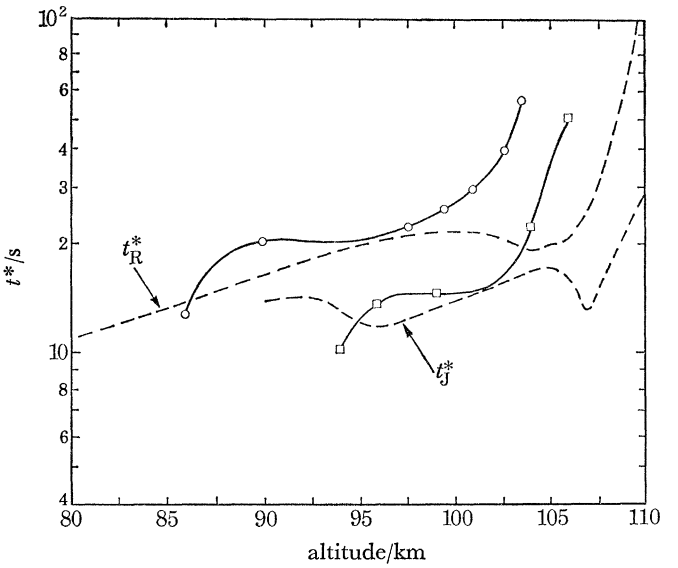

FIGURE 7. Variation with altitude of the time constant of the Kolmogoroff microscale (– – –). Also delay in onset of turbulence: ○, SL 761 (morning); □, SL 762 (evening).

PHILOSOPHICAL TRANSACTIONS OF THE ROYAL SOCIETY A MATHEMATICAL, PHYSICAL & ENGINEERING SCIENCES

TABLE 4. VARIATION WITH ALTITUDE OF THE CONSTANTS OF THE KOLMOGOROFF MICROSCALE (AFTER JUSTUS 1967*b*)

altitude / km	ϵ_J / W kg^{-1}	t_J^* / s	η_J / m
90	0.031	13.3	53.6
91	0.035	13.6	59.0
92	0.040	13.9	64.9
93	0.050	13.5	69.7
94	0.070	12.4	72.8
95	0.10	11.3	75.6
96	0.13	10.8	80.4
97	0.14	11.3	90.0
98	0.15	11.9	100
99	0.16	12.6	112
100	0.17	13.3	125
101	0.18	14.0	140
102	0.19	14.9	157
103	0.20	15.6	173
104	0.22	16.4	195
105	0.25	16.7	215
106	0.36	15.2	223
107	0.63	12.5	220
108	0.44	16.3	274
109	0.30	21.4	342
110	0.20	28.6	430
111	0.13	38.7	544

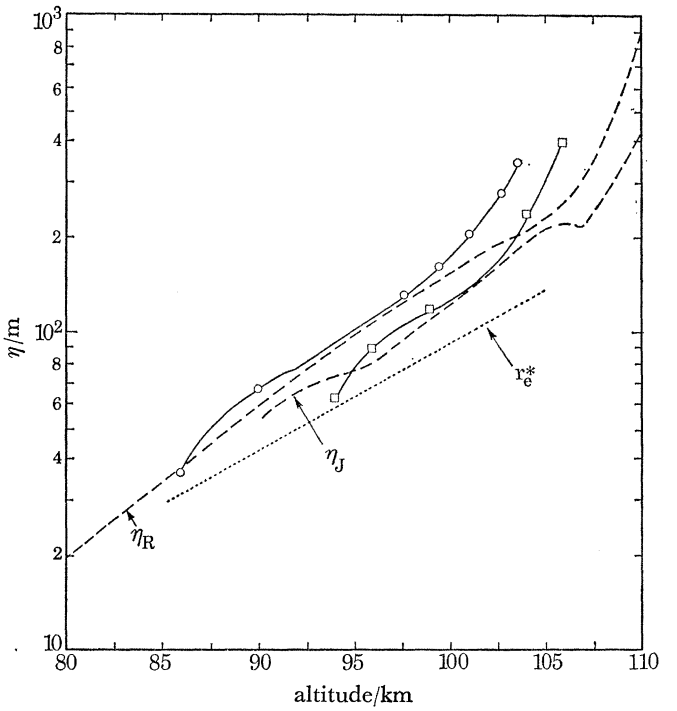

FIGURE 8. Variation with altitude of the Kolmogoroff microscale (– – –). Also inferred microscale: ○, SL 761(morning); □, SL 762 (evening).

at best approximate above 80 km; (*b*) the variation, both diurnal and seasonal, in the turbulent dissipation rate which has been averaged out in the construction of the t^*_R and t^*_T profiles; and (*c*) the fact that, while the parameter t^* appears to be a measure of the time taken for trail break-up to occur, it is not clear why it should be.

The definition of η is only a mathematical expedient characterizing the spectrum of scale sizes responsible for the viscous dissipation. There is no obvious reason why either η or t^* should be physically measurable features of the motion. Nevertheless, the close similarity in the shapes of the t^* curves, which all show a flat region followed by a sharp rise, strongly indicates that the time delay in the onset of turbulence should be related to the time constant of the Kolmogoroff microscale. Furthermore, these observations suggest a reason why the turbopause, defined as the boundary between the region which breaks up and that which remains laminar, should manifest itself so abruptly. Attempts have been made to explain the existence of the turbopause in terms of a critical value of some parameter, generally the Reynolds number or the Richardson number (see, for example, Blamont & Barat 1967*a*). These attempts have met with little success, partly because of the difficulty in defining the characteristic lengths which occur in these parameters and partly because it is not evident, *a priori*, what value the parameter should have at the turbopause. The error which has often been made is in assuming that the turbopause corresponds to an altitude at which turbulence ceases abruptly. Our results, on the contrary, show that the turbopause is the altitude at which the time constant of the Kolmogoroff microscale of the turbulence increases very rapidly with altitude. This viewpoint resolves the paradox that regions above the turbopause, which were thought of as non-turbulent, have a diffusion coefficient which is greater than molecular. We now see that turbulence does exist above the turbopause, but, as is shown by the diffusion results, its efficacy in transport processes, relative to molecular diffusion, decreases with altitude. At a mean altitude of 130 km, the contribution by turbulence is insignificant, even though its absolute value may be as large as it is at the turbopause. It is pertinent to mention here that, unlike Müller (1968), we have not differentiated between random internal waves (gravity waves) and turbulence, subscribing to Lumley's (1964) definition of turbulence as 'any random, three-dimensional velocity field with a continuous spectrum, displaying spectral transfer and dissipation at high wave numbers', which includes the case of internal waves. Part of the justification by Hines (1960) of his random internal atmospheric gravity wave theory lies in his identification of the oft reported '7 km vertical, 150 km horizontal scale' (associated with the short-period departures from the mean motion at meteor heights) as the 'dominant mode' of the gravity wave spectrum at these altitudes. Roper (1966*a*) has shown, by extrapolation from small-scale shears (< 3.5 km length scale), that conventional turbulence theory would predict a régime of energy-bearing eddies of identical dimension to the 'dominant mode' gravity wave, thus confirming Lumley's definition.

The duality is not, however, complete. One does not talk about the propagation of turbulence through the atmosphere, whereas gravity waves can propagate. Once the motion spectrum has contracted to the point where the mechanism of energy loss can be described as viscous damping without a cascade of energy down through smaller scales, then the term 'viscous dissipation of gravity wave energy' replaces the 'turbulent dissipation' which is characterized by small-scale motion, and is therefore responsible for the 'obviously' turbulent nature of vapour trails below the turbopause. In emphasizing the nature of the turbopause in the preceding discussion, we have used the word 'turbulence' to describe dissipation above the turbopause, whereas 'viscous damping of gravity waves' is a more appropriate term. Whether or not one can distinguish

between a broad spectrum of internal atmospheric gravity waves and turbulence depends on the measurements taken. If one can continuously monitor the wind velocity, temperature, pressure and/or density, discrimination between gravity waves and turbulence is easy. When only the wind field is monitored, and that only for a short period of time, as is the case in our experiments, difficulties in interpretation arise.

Because of the chaotic nature of the break-up of the Skylark trails, the only parameter which could be sensibly measured was the delay in the onset of turbulence. Since this delay time appears to be the characteristic time of the Kolmogoroff microscale (which depends only on ϵ and ν), ϵ can be calculated, assuming ν as previously calculated from the *U.S. Standard Atmosphere Supplements* (1966). The turbulent dissipation rate profiles appropriate to the morning and evening trails are presented in figure 9.

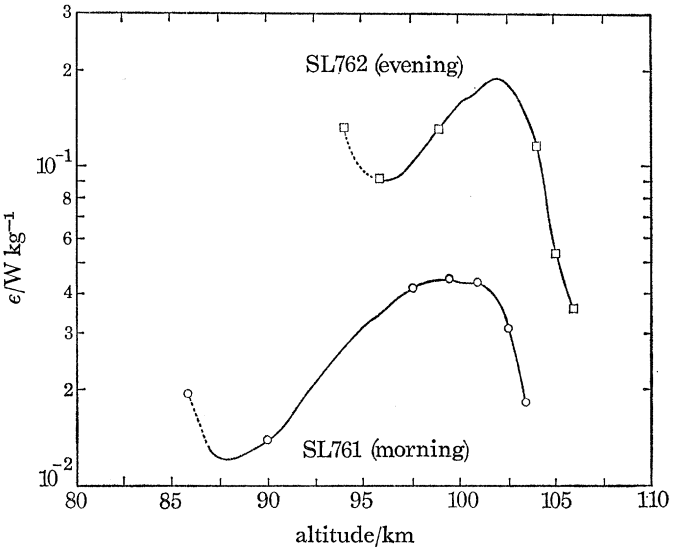

FIGURE 9. Profile of the turbulent dissipation rate.

The rate of dissipation of turbulent energy can also be calculated from the rate of expansion of the trail after eddy diffusion becomes effective. Several authors have applied the equation

$$r^2 = \tfrac{4}{3}\epsilon t^3, \tag{4}$$

derived by Booker & Cohen (1956) to this problem. This equation, as originally pointed out by the authors, is only valid at times, t, much greater than the time constant of the smallest eddies. The complete equations derived by Booker & Cohen were

$$r_t^2 = 4Dt + r_0^2 \tag{5}$$

applicable to the region of molecular diffusion with coefficients D and initial trail radius, r_0; and

$$r_t^2 = \tfrac{4}{3}\epsilon(t^3 - t_2^3) - r_2^2, \tag{6}$$

for the turbulent régime, where the suffix 2 denoted the transition from molecular to turbulent diffusion. It should be noted that equation (5) defines r_t as the effective radius r_e, as used in this paper, and not as the Gaussian radius as has often been assumed by others.

Substitution of the time-dependent behaviour of r_e^2 at 105 km from figure 6 into equation (6) yields

$$\epsilon = 0.37\ \mathrm{W\,kg^{-1}},$$

which is six times greater than the dissipation inferred from the time of onset of turbulence. Similar discrepancies between estimates of turbulent dissipation based on different parameters measured from chemical releases in the upper atmosphere have been reviewed by Zimmerman (1966*a*). We agree with the emphasis he places on the careful assessment of what is really being measured.

We have already shown that our morning and evening trails reached observable diameters much larger than the Kolmogoroff microscale before breaking up. The effective radius r_e at the time of onset of turbulence in figure 8 is seen to be of the same order as the inferred microscale η, but, since $\epsilon \propto \eta^{-4}$, minor discrepancies are highly significant. While our measurements of r_e, as presented in figure 6, qualitatively describe the behaviour of the trail, at no time was the trail radiance profile truly Gaussian, and so we have based our turbulence dissipation rate profiles on our well-established time constants, rather than the length parameters, whose measurement is in doubt.

We will now discuss the implications of the deductions which we have made. Figure 9 shows not only that the atmosphere below the turbopause is more turbulent in the evening than in the morning, but also that the turbopause is higher in the evening. If this measured correlation applies also to the semi-annual variation in turbulent intensity found at 93 km by Roper & Elford (1963) from meteor trail results, then weight is given to the semi-annual variation in turbopause height suggested by Elford & Roper (1967). This suggestion is also supported by the rocket-borne mass spectrometer measurements of diffusive separation published by Meadows & Townsend (1958, 1960) which, although measured at the much higher latitude of Fort Churchill, Canada, indicate a lower turbopause in November 1956 than in February 1958, a variation which is in phase with Roper & Elford's (1963) semi-annual variation in turbulent intensity at 93 km. We also think that the diurnal, and by inference, the semi-annual variations in turbulent intensity and turbopause height are the 'meteorological mechanism' invoked by Sullivan & Roberts (1968) to explain their measurements of both diurnal and semi-annual variations in the height of the twilight sodium layer.

Johnson (1967), Cook & Scott (1967) and Justus & Roper (1968) have all commented on the correlations between various aspects of the dynamics of the turbopause and the density at satellite heights, first discussed by Kochanski (1963, 1965). While the semi-annual variation in turbopause dynamics and in densities at much higher altitudes both have their source in the solar output, it does not follow that turbopause dynamics and high altitude densities have a causal dependence; i.e. it does not mean that the energy input to the magnetosphere propagates down and affects the turbosphere, or that energy input to the lower atmosphere propagates upward into the thermosphere. The time scale of the variations is long, and it is quite probable that input to the magnetosphere increases the density at the same time as input to the lower atmosphere increases the dynamical energy of the lower thermosphere. Our density measurements indicate a decrease in density in the lower thermosphere with increase in turbopause height. Thus increase in turbopause height does not necessarily mean an increase in density immediately above the turbopause (at least, not on a diurnal time-scale), even though the diurnal variation in satellite density is in phase with our measured turbopause height variation (*U.S. Standard Atmosphere Supplements* (1966)).

We have already discussed at some length the turbulent dissipation of wind energy below the turbopause, and the viscous dissipation above. Hines (1965) has semi-empirically estimated an average viscous damping rate profile which follows smoothly on from the average turbulent

dissipation rate profile estimated from the same data by Roper (1966*b*); this shows that *on average*, viscous dissipation is as effective as turbulent dissipation. However, for any given gravity wave system propagating vertically through the lower thermosphere, the heating due to viscous damping above the turbopause may be less than that due to turbulent dissipation below, because of the depletion of energy from the wave spectrum as it passes through the turbulent region, assuming that the gravity wave spectrum is generated at lower altitudes (Hines 1965). Even if the gravity wave spectrum is generated *in situ* in the 80 to 100 km region by the diurnal tide, as proposed by Roper (1966*a*), this argument still holds, in that the amount of gravity wave energy propagating from the region of generation could still be considerably less than that which is being turbulently dissipated.

If the turbulent dissipation of wind energy below the turbopause is greater than the viscous dissipation above, then there should be greater dynamical heating of the atmosphere at the level of maximum dissipation of turbulent energy, with a consequent modification of the temperature profile. Such a modification has been observed at 106 km in a temperature profile measured by Wand & Perkins (1968) using the Thomson scatter radar at Arecibo (5° N). On the basis of our mid-latitude observations, we agree with their first suggestion, that the energy source responsible for their temperature maximum at 106 km is dynamical heating by gravity wave dissipation, or, more correctly, turbulent dissipation of gravity wave energy, rather than the reversible heating by tidal wind oscillations, as elaborated on by Hooke (1969). It should be noted that we believe the almost adiabatic decrease in temperature to the 113 km level is the result of turbulent mixing (Lloyd *et al.* 1972), and does not indicate an energy sink at that level.

The source of the turbulent energy

In a stably stratified region, such as the lower thermosphere, it is generally accepted that the source of turbulent energy is wind shear. Several authors, notably Blamont (1961, 1963), Blamont & Barat (1967*a*), Zimmerman (1966*b*), Hodges (1967) and Rosenberg (1968*b*) have attempted to explain the generation of turbulence below, and its cessation at, the turbopause in terms of either the Reynolds or the Richardson numbers, or both. All have had some difficulty in deciding on critical values for these numbers, except for Hodges, whose results can be applied to show that the alternation of laminar and turbulent regions reported by Blamont & Barat (1967*b*) could result from the Richardson number actually becoming negative and the atmosphere superadiabatic at the wind shear minima.

Temperature measurements of the neutral atmosphere in the neighbourhood of 100 km have been made by Brandy (1964, 1965) and Blamont & Lory (1964), but such observations are far from routine; in particular, little is known of the diurnal and seasonal variations of the temperature profile at these heights. Unfortunately, we have temperature measurements in the lower trail for the morning release only (their determination is treated in the section on temperature from shock wave propagation). While the mean temperature profile from four points can hardly be regarded as significant, it does indicate that the upper level of the mesopause lies at about 98 km, which is the height of the maximum in the morning turbulent dissipation rate profile. This is in keeping with Lumley's (1964) assertion that 'any energy imported into, or produced in, a temperature inversion, will excite a quite intense band of internal waves at low wavenumbers, in addition to an inertial and viscous field at high wavenumbers'.

While one should always bear in mind the fact that the efficacy of wind shear as a source of turbulent energy depends intimately on the temperature profile, the wind shear profile is at least a measure of the energy available for possible dissipation. Since shear stress is responsible for the vertical correlation of the wind profile, the estimate of the shear at a given altitude must take into account this vertical correlation. This is done in the formation of the structure profile, S (Kolmogoroff 1941), which, when applied to the measured mean wind profile, U, may be expressed in its time independent form as

$$S(\Delta h) = \langle [U(h) - U(h+\Delta h)]^2 \rangle,$$

where the average is taken over a height range at least equal to the vertical correlation distance.

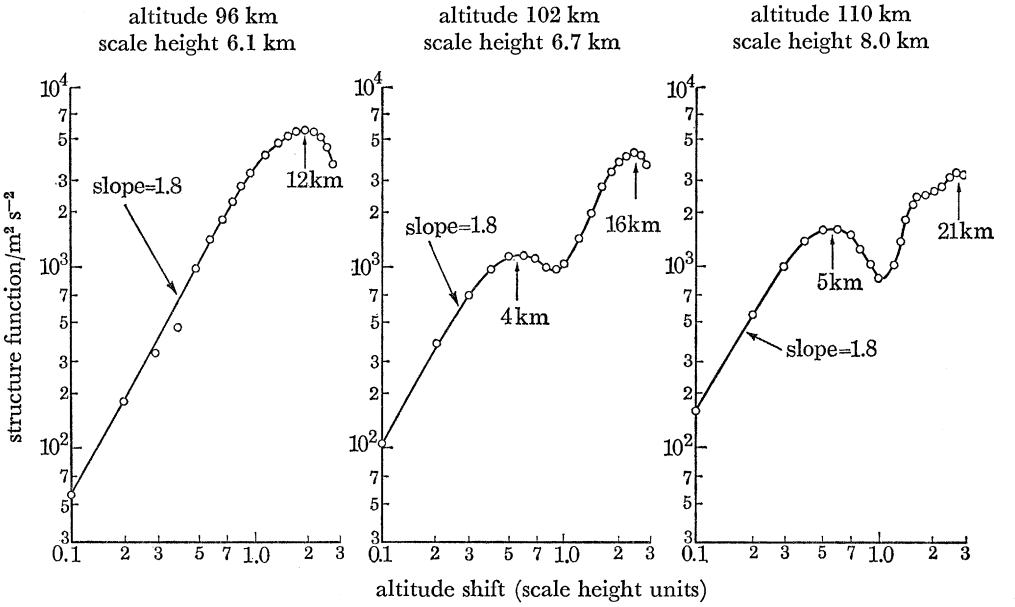

FIGURE 10. Structure function from morning wind profile.

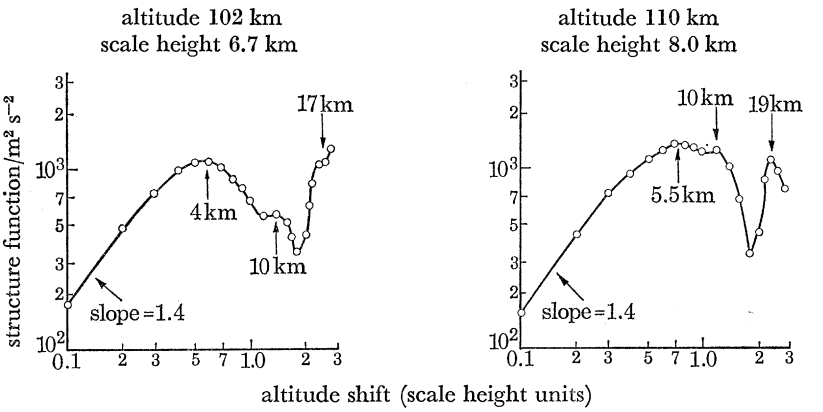

FIGURE 11. Structure function from evening wind profile.

The structure functions calculated from the measured total wind speed profiles of the regions centred on 96, 102 and 110 km (i.e. 3, 4 and 5 scale heights above 80 km) for the morning trail are presented in figure 10, and those centred on 102 and 110 km for the evening trail in figure 11. Since the evening trail did not start until 92 km, no estimate of the structure function at 96 km was possible.

Since the wind shear magnitudes for the firings correlate negatively with the rate of dissipation of turbulent energy, while the structure functions are qualitatively appropriate, we can only assume that the temperature profile, of which we have no knowledge in the evening, is the criterion which determines stability. The fact that our measured evening wind profile departs significantly from the evening mean meteor wind profile (figure 2) could be interpreted as indicating a much larger contribution to the wind energy by random winds (internal atmospheric gravity waves/turbulence) in the evening. However, large phase anomalies in the tidal meteor winds have been measured in a day-by-day survey by Doyle (1969), and these could equally well be responsible for the departure of our measured evening profile from the meteor wind mean. Of course, such phase anomalies could 'equally well' be associated with the instability in the diurnal tide proposed by Lindzen (1968) which 'leads to the generation of short time and space motions in the form of gravity waves and/or turbulence'; on the other hand, the breakdown of the diurnal tide may be caused by the influx of gravity wave energy into the meteor region, as proposed by Spizzichino (1969). Our measurements do not enable us to completely resolve the effect, let alone the cause.

Shock wave temperature determination

Attempts to observe the propagation of shock waves created in the upper atmosphere above about 90 km altitude have been made on several occasions during the past few years; see, for example, Blamont & De Jager (1961) by detonation of a large amount of pyrotechnic explosive from a rocket payload, Stoffregen (1968) from the detonation of high explosive in aurora, Rosenberg (1964) and Rees (1967) by release of HEX grenades in a TMA trail carried by the same rocket.

Observations have mainly relied on framing cameras (Blamont & De Jager 1961) or a streak camera principle (Rosenberg 1964; Rees 1967), where the film is moved uniformly, and approximately perpendicular to the projection of the rocket trajectory on the film. In addition, Rees (1967) has used photoelectric detectors incorporating a graticule of clear, parallel lines placed in the image plane of a telephoto lens.

During the Woomera experiments, a streak camera and three photoelectric detectors were used to observe the detonations of four HEX grenades released between 90 and 135 km on both the TMA trails. An additional experiment was attempted by exploding charges of 5, 20 and 40 kg of high explosive at ground level some 5 to 6 min before the rocket launch (see table 5). The intervals between the detonations and rocket launch were calculated to allow the rocket to overtake the shock waves at the altitudes shown in table 5.

Table 5. Detonation times of ground explosions

mass of explosive	altitude/km at which rocket overtakes shock		time of detonation	
kg	calculated	observed	before launch/s	overpressure/%
5	120	not detected	−320	—
20	110	100 to 102	−295	*ca.* 3
40	100	97 to 98	−260	*ca.* 10

A montage of a streak camera photograph, its isodensitrace, and a Baker Nunn photograph, from the morning firing, are shown in figure 12, plate 10. In the streak photograph the grenade shock waves appear as low-contrast hyperbolic features extending from the grenade into the TMA

trail 'smear' and are adequate for an approximate analysis by means of the isodensitrace. The measurements of velocity were made from initial coordinate measurements obtained by projection of a high key positive transparency on to a high contrast print. In this way the contrast of the shock wave features is greatly enhanced. For comparison, the data was also analysed using a microdensitometer with paper-tape output attachment for computer analysis. The results of this second method agreed well with the first and gave an indication of the probable error.

The third presentation in the montage is two polaroid photographs of a television screen where the video signal of the television has been electronically modified on an isodensitrace principle, with the intention of separating the shock wave features by a single high-density increment from the 'plateau' of the background TMA emission.

The two rather broad, faint features labelled on the isodensitrace are believed to be due to the effects of two of the ground detonations. These shock waves will propagate upwards through the atmosphere and, even allowing for the entropy effects (Groves 1963), it is found that the overpressure of the wave is greatly enhanced in regions above 60 km owing to the necessity of maintaining a constant energy flux as the atmospheric density decreases. The basic structural similarity of the shock waves from the largest ground explosion, and the lowest grenade shock wave, in width, overpressure, period of detectability and velocity, can thus be most readily demonstrated.

At 98 km, the mean altitude of the lower feature, which is due to the latest and largest explosion, the overpressure of the wave should, theoretically, be approximately 5 %. This is in relatively good agreement with the observed intensity increase of about 10 %. The rise to maximum intensity of the feature, over about 800 m, is mainly due to the combination of the diameter of the trail, Gaussian radius 300 m at 20 s after release, and the aspect angle from the observation site. The theoretical leading edge thickness of a shock wave at this altitude is only a few metres.

Observations on the shock waves were slightly hindered on the morning release (at 12° solar depression angle) by the background sky intensity. The shock waves were not observed at all in the evening (at 9°) when the sky brightness was higher than expected.

TABLE 6. STREAK CAMERA DATA

	altitude / km	mean alt. of measurement	velocity/m s^{-1} corrected for wind and Mach no.	T/K
grenade 1 (up-wave)	93.25	94.0	258 ± 20	160 ± 40
ground shock wave 3	97.0	98.0	250 ± 20	160 ± 40
ground shock wave 2	100.3	101.0	280 ± 20	190 ± 40
grenade 2 (up-wave)	102.6	103.6	310 ± 20	240 ± 30

The velocities of all four shock wave features were corrected for the effects of ambient wind velocity, and also for the Mach number of the shock waves (Rees 1967); values for temperature were calculated from the corrected shock wave velocities using CIRA 1965 data for the mean molecular weight and for calculating γ, the ratio of the principal specific heats (Rees 1967). Table 6 gives the observed velocities and derived temperatures.

Spectral observations

The spectra of the clouds were obtained to give information on the constituents of the glow clouds and their lifetimes, and to derive the ambient temperature at the clouds. Before discussing these aspects, brief mention of the spectrometers will be made.

Three instruments were used to determine the spectra of the clouds – the W.R.E. spectroradiometer described by Johnson (1968), the U.C.L. spectroradiometer described by Rees (1968) and an echelle spectrograph. Although the construction of the latter instrument has been described by P. R. Gillingham (1969, private communication), and its use to determine temperatures from AlO glow clouds by Roper & Low (1969), the high resolution of this instrument, and its sensitivity, warrant a brief description here.

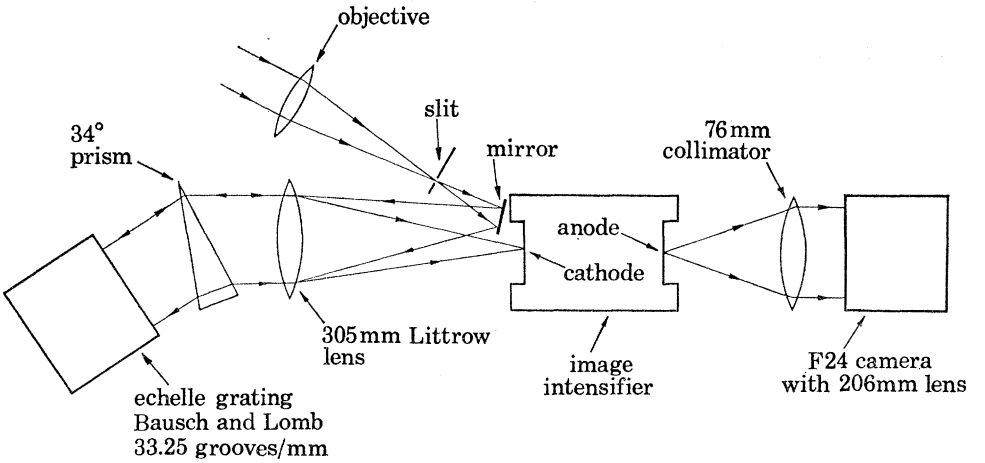

Figure 13. Schematic diagram of the echelle spectrograph.

A schematic diagram of the echelle spectrograph is given in figure 13. Light from the cloud which enters the system is dispersed by an extra dense flint prism placed in front of an echelle grating in a Littrow mounting. The dispersions of the prism and grating are crossed. This means that high dispersion over a wide range of wavelengths is possible without overlapping orders. For example, the 51st order of 500 nm and the 50th order of 510 nm, which would normally overlap one another, now lie one below the other. The instrument is designed so that at 380 nm the 62nd order passes through the optical system, and at 720 nm the 34th order passes through the system. After the dispersing elements, the light falls on to the photosensitive cathode of an image intensifier tube. An F 24 camera photographs the final anode image on the tube. The spectrograph has an integrating photometer built into the light path which indicates when the frame has been sufficiently exposed. Since the system uses both image intensification and photographic techniques, intensity calibration is difficult. However, as only relative intensity levels are required for the determination of temperature from the AlO band spectra, by careful checking against standard sources satisfactory accuracy has been obtained.

Figure 14, plate 11, shows the echelle F 24 camera photograph of a glow cloud spectrum. A barium II line at 493 nm is marked. This is one of the barium lines which give rise to the errors in the diffusion coefficient at high altitudes; in this instance it serves an extremely useful purpose. To relate the theoretical AlO band profiles to the experimentally determined ones, it is necessary to include the smoothing caused by the slit function. Although in theory this may be calculated, in practice it has been found to be very sensitive to the setting of the instrument, and to vary

PHILOSOPHICAL TRANSACTIONS OF THE ROYAL SOCIETY A MATHEMATICAL, PHYSICAL & ENGINEERING SCIENCES

from trial to trial. It is, therefore, necessary to determine the slit function experimentally, preferably under identical conditions to those under which the experimental observations are being made. Since the slit function is defined as the output produced by scanning a line, and since the slit function can vary with wavelength, a spectral line such as the Ba II line, which is located midway between the two strongest bands of the AlO spectrum, is ideal.

We will now describe the spectral features of the glow clouds, and discuss their significance. The grenades which are used to produce the glow clouds contained aluminium powder, potassium perchlorate and barium nitrate (Armstrong 1963). They were all released in sunlight above the Earth's shadow. Each cloud resonantly emitted AlO band spectra; in addition, the Al I lines at 394.4 and 396.1 nm, and the K I lines of 404.4, 404.7 and 769.9 nm appeared on all scans that covered these regions of the spectrum. Johnson & Low (1967) reported the Al line at 308.2 and 309.3 nm; however, it now appears that this identification was in error and that these features are the violet system of AlO $B^2\Pi$–$X^2\Sigma$ (see Johnson & Low 1967, Figure 1).

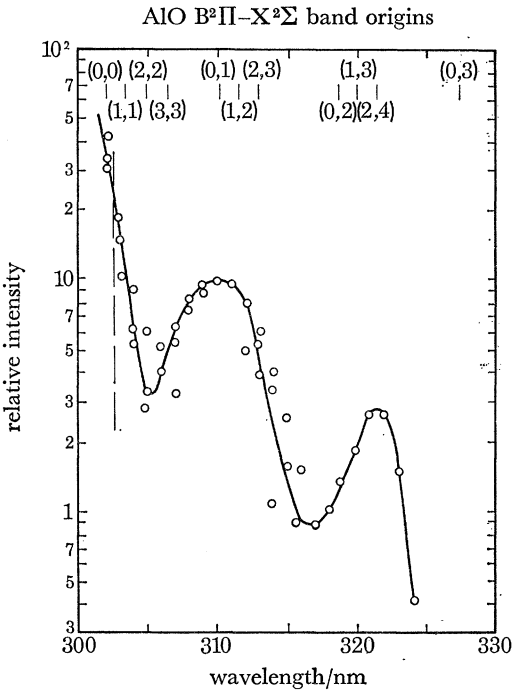

FIGURE 15. Relative intensities in the $B^2\Pi$–$X^2\Sigma$ band system. Data below 303 nm are very unreliable because of the rapid change in ozone absorption with wavelength.

Figure 15 shows the $B^2\Pi$–$X^2\Sigma$ band system of AlO from a glow cloud at 186 km released from a firing in October 1963. The figure was constructed from several spectra at 5 nm resolution in order to reduce the noise level; the observations have been corrected for atmospheric transmission, and for instrument sensitivity. This band system is not normally observed because the atmospheric absorption at 310 nm is very strong. In only a few firings have the glow clouds been far enough above the Earth's shadow for the Sun's radiation, reaching the cloud at these wavelengths, to be sufficiently intense to give a reading on the instruments, which are rather insensitive at 310 nm. The $B^2\Pi$–$X^2\Sigma$ band systems were not detected on the two firings reported in this paper, even though some of the clouds were far above the Earth's shadow, because most scans were limited to the $A^2\Sigma$–$X^2\Sigma$ band system. The few early scans over the complete spectrum were taken at 1.6 nm

resolution, for which the instrument throughput is only a tenth of that at 5.0 nm resolution. At late times the $B^2\Pi$–$X^2\Sigma$ band system is too faint even to be observed at 5.0 nm resolution.

We are confident in the identification of this feature (310 nm) with the $B^2\Pi$–$X^2\Sigma$ band system of AlO, because of the agreement between the position of the bands with the origin values calculated using the vibrational and rotational constants for the electronic states given by Goodlet & Innes (1959) and Lagerquist, Nilsson & Barrow (1957), and the head values given by Becart & Declerck (1960). The band system was a third as bright as the $A^2\Sigma$–$X^2\Sigma$ system. If we allow a factor of 5 for the difference in the Sun's irradiance at these wavelengths, the f values for the corresponding transitions have about the same value, which Johnson *et al.* (1967) found to be 0.005. We have never observed the red $B^2\Pi$–$A^2\Sigma$ band system of AlO. The reason that it was not even observed from the 196 km cloud in October 1963, when we might have expected to see it, is almost certainly due to the ν^3 reduction in the transition probability between electronic levels.

Johnson & Low (1967) observed that twilight releases radiated a continuum, as well as the AlO, Al and K emissions described above. This continuum had the same distribution as that observed from grenade glow clouds at night, or in the Earth's shadow. The present results do not show this continuum, probably because these glows were formed above the region where night-time emissions would persist.

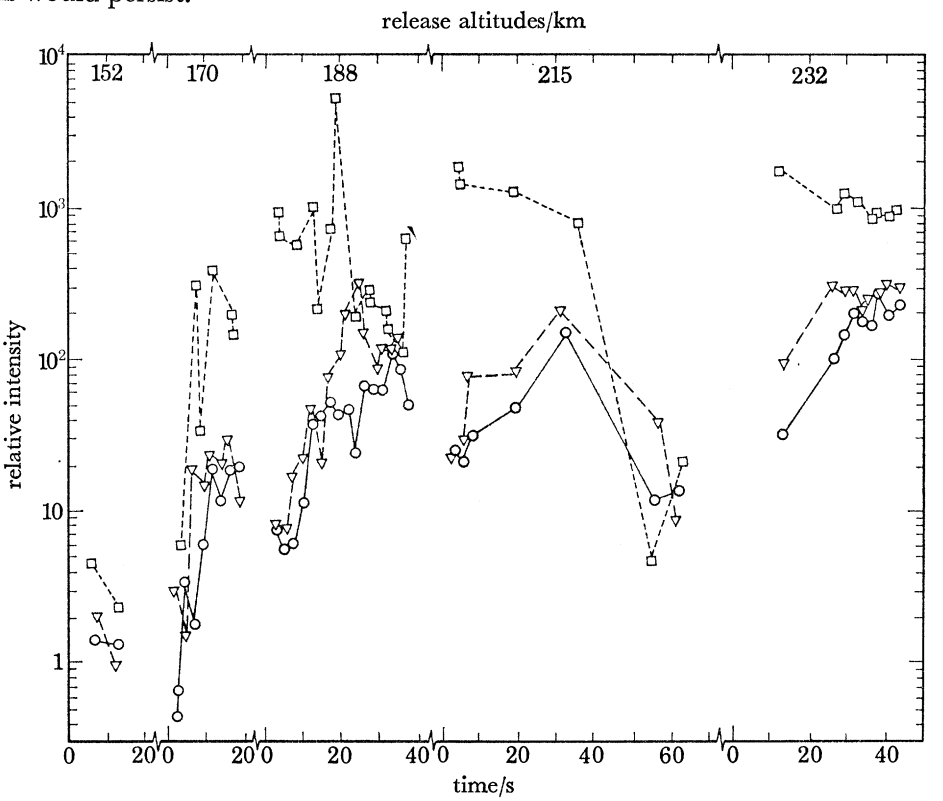

FIGURE 16. Variation of Ba I and Ba II line intensities. ▽, Ba II, 455.4 nm; ○, Ba II, 493.4 nm; □, Ba I, 553.5 nm.

The barium in the grenades also resonantly scatters sunlight: the brightest line was the Ba I line at 553.5 nm, but the Ba II lines at 455.4 and 493.4 nm were also recorded in all glows. Features corresponding to barium lines in the wavelength range 580 to 730 nm were also recorded. A feature at 852.5 nm which appeared on a few spectra at 243 km altitude in the morning and

persisted for at least 60 s could be the Ba 852.2 nm line. The other lines between 580 and 730 nm decayed more rapidly. The appearance and persistence of Ba at 553, 493 and 455 nm is altitude dependent. Johnson, Lloyd, Low & Sheppard (1967) reported that the 455 nm line decayed rapidly, even at 157 km. We must now point out that this is incorrect; the behaviour described was in fact that of the 553 nm line. Figure 16 shows the behaviour of the barium line intensities, relative to that of the AlO bands; this gives a measure of relative concentration of barium species, as the number of AlO molecules does not markedly vary with time at these altitudes.

There seems to be an anti-correlation between the continuum and the barium line intensities: at altitudes below about 150 km the continuum is strong and the barium radiations decay rapidly; at higher altitudes there is no continuum and the many barium lines persist; at yet higher altitudes, above about 200 km, only Ba II lines are observed. This behaviour can be explained in terms of the atomic oxygen profile if we assume, as suggested by Johnson *et al.* (1967), that atomic oxygen is responsible for the glow cloud continuum. At lower altitudes, at which atomic oxygen density is larger, the chemiluminescent reaction occurs at a rate sufficient to produce an observable continuum, and the barium is rapidly oxidized to BaO. At higher altitudes the atomic oxygen density is not sufficient for this oxidization. At the highest altitudes Ba II is produced by photoionization of the Ba I 6s 5d ^{1}D metastable state by 326 nm photons (Föppl *et al.* 1967), and the intensities of the Ba I lines fall.

For many years we have kept records of the duration (defined as the time after release at which the radiance of the glow cloud has fallen to a given level) of glow clouds as a function of altitude.

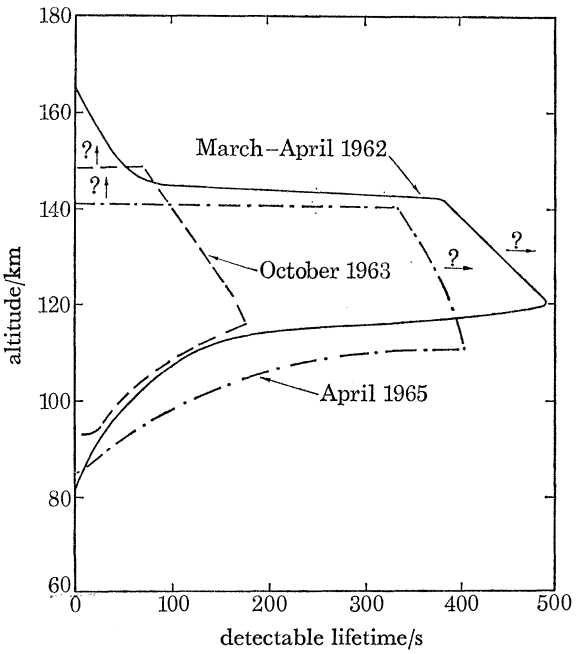

FIGURE 17. Lifetime envelope of the chemiluminescent emission.

Figure 17 shows the altitude regions in which the continuum was observed. It is seen that there is a flat peak, and the lifetime falls quickly at altitudes above and below this peak. There is definite vertical movement of the envelope of the glow cloud lifetime over the years; the results of the Skylark firings SL 363, 364, 462, 463 and 464 (April 1965) also indicated that the envelope drops during the night.

The shape of the profile, and its movements, can be explained by consideration of the atmospheric O_2 and O profiles. There are three regions involved in producing continuum spectra. At the lowest level there is plenty of contaminant, but it is rapidly consumed by reaction with atmospheric oxygen (both O_2 and O) and oxygen provided by the explosion products, because the relatively higher pressure, and hence lower diffusion coefficient, keeps the explosion products in relatively close contact. As the altitude increases, the pressure decreases and the life of the glow is determined mainly by the reaction with atomic oxygen, with a small contribution from diffusion. A balance is then reached between the effect of diffusion and atomic oxygen concentration and the glow clouds persist for a few hundred seconds. Finally, at still higher altitudes the glows are not recorded because of the low reaction rate due to the decreasing atomic oxygen density and increased diffusion coefficient.

The vertical movement on the envelope of the glow cloud lifetime suggests that the profile of the atomic oxygen distribution also varies; in particular, the fall in the profile during the night indicates that, as one would expect, the atomic oxygen density decreases during the night.

Figure 17 shows a seasonal behaviour of the lifetime of the clouds, which may also be assumed to represent a seasonal variation in atomic oxygen densities. Not much is known about the seasonal dependence of the atmospheric structure, because the mass spectrometer experiments have generally been planned to study diurnal variations. However, the calculations of Colegrove, Johnson & Hanson (1966), which show that the atomic oxygen profile is sensitive to the eddy diffusivity, and the observations of Elford & Roper (1967), who find a seasonal variation in the rate of dissipation of turbulent energy, together predict a seasonal variation. Our observations do not warrant a quantitative analysis; they do no more than suggest a seasonal behaviour.

Temperature from AlO band spectrum

The intensity distribution in the resonant AlO band spectrum depends on the temperature (Authier *et al.* 1962). If one assumes that collisions between the ambient atmosphere and the AlO molecules are sufficiently frequent for the rotational and vibrational levels of the AlO molecules in the ground state, $X^2\Sigma^+$, to have a Boltzmann distribution corresponding to the temperature of the ambient, then it is possible to compute theoretically the band profile at any given temperature (Harang 1967; Low 1967). The brightest resonant bands of the AlO molecule are the $A^2\Sigma^+$–$X^2\Sigma^+$ system, and these are invariably used. The temperatures were determined as follows. The raw data was processed using the wavelength, wavelength sensitivity including atmospheric extinction, and intensity calibrations of the instruments, to produce an intensity *vs.* wavelength plot of the sequences required. This was compared with a similar synthetic plot produced from the molecular constants, incident solar flux including corrections for the absorption of Fraunhofer lines (see later), transition probabilities and instrument slit function. Particular care was taken to obtain several spectra over the longest possible period from the clouds over 200 km altitude by means of all three instruments. The data, in particular that from the echelle spectrograph, were examined for the vibrational temperatures indicating insufficient collisions between resonant excitations, with a corresponding rise in temperature with time. The observed spectra did not show this effect.

We shall now give some consideration to overall accuracy. The data in figures 18 and 19 come from three different instruments; two are grating spectroradiometers; the third is an echelle spectrograph. The U.C.L. spectroradiometer has a resolution of 0.3 nm and records on a linear

scale. The signal currents used are much greater than the detector photomultiplier dark currents. There is sufficient electronic smoothing for the shot noise of the photomultiplier to be smoothed in the output trace.

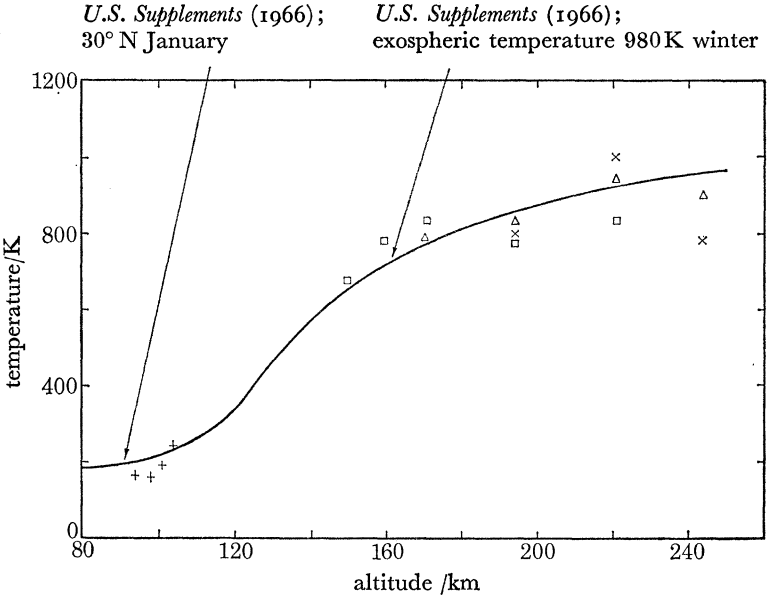

FIGURE 18. Morning temperature profile. From AlO spectra: △, echelle spectrograph; □, U.C.L. spectroradiometer; ×, W.R.E. spectroradiometer. +, from shock wave.

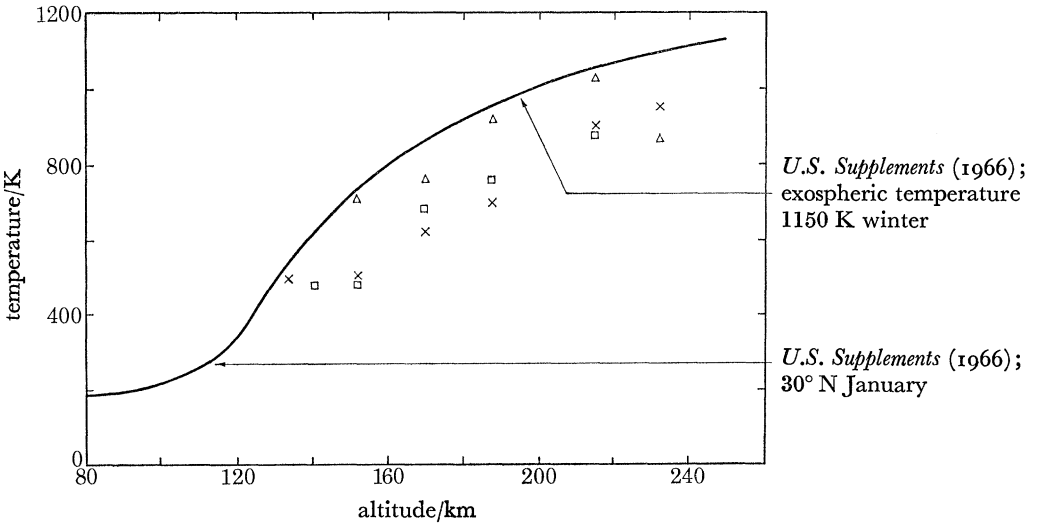

FIGURE 19. Evening temperature profile. From AlO spectra: △, echelle spectrograph; □, U.C.L. spectroradiometer; ×, W.R.E. spectroradiometer.

The analogue output was also recorded in F.M. mode and analysed later by computer via an analogue-digital converter on to paper tape. Manual and computer matching of observed and computed spectra generally agreed within 50 K, while differences of less than 20 K were detectable in the computer-matching of observed spectra with the computed smoothed spectra (figure 20). Owing to unknown, but probably small, systematic errors, the standard deviation for this method is around 50 K, though the results are consistent to better that this. Figure 20

compares a spectrum, reduced from our observations, with a synthetic spectrum which has been appropriately smoothed, for various temperatures. The difference between the left- and the right-hand spectra is due to the asymmetric effects of the amplifier and the oscillatory spectrum scanning system. This particular spectrum is a left-hand one and should be compared with the '1' synthetic spectrum.

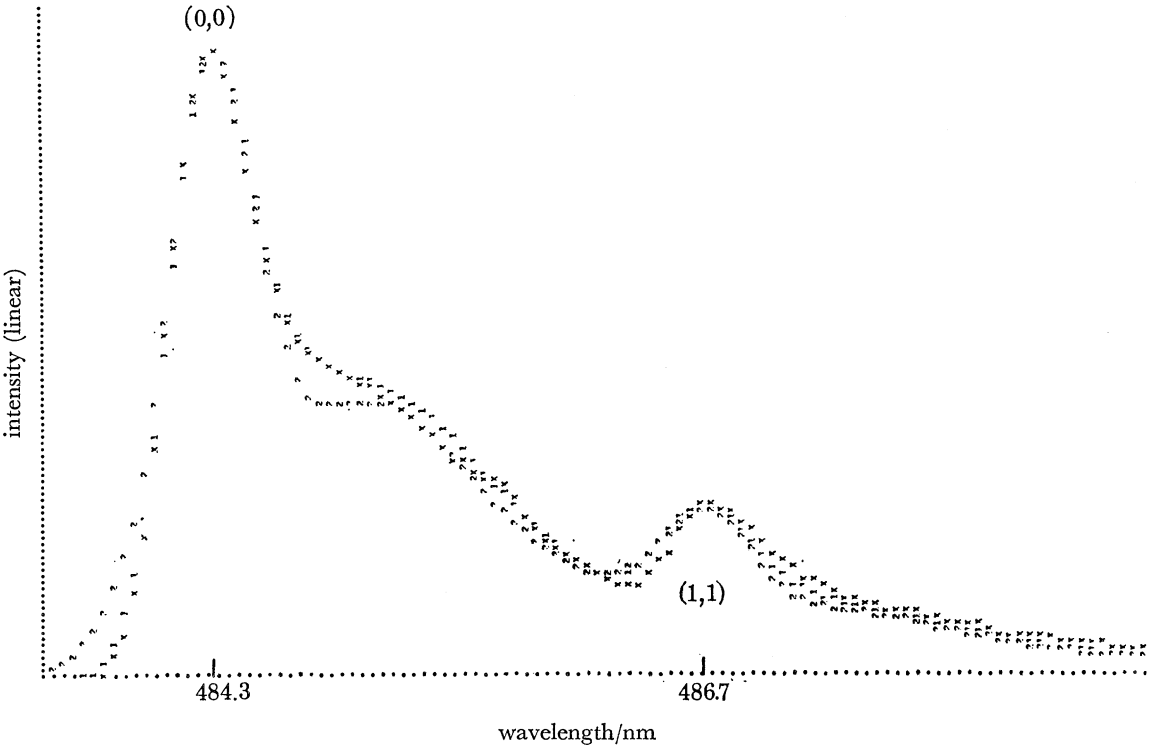

FIGURE 20. Comparison of observed and theoretical spectra. ×, observed; 1,2, synthetic (see text).

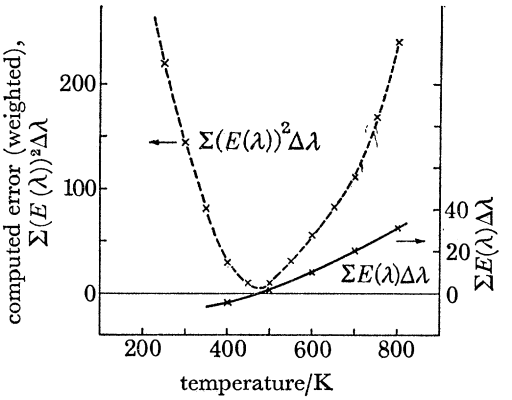

FIGURE 20 (*a*). Plot of computed errors of observed spectrum against temperature. AlO spectrum SL 762; time after launch 156 s; altitude 153 km. $\Sigma\{E(\lambda)\}^2\Delta\lambda = \Sigma[W(\lambda, T)\{I_{obs}(\lambda) - I_{syn}(\lambda, T)\}]^2\Delta\lambda$; $\Sigma E(\lambda)\Delta\lambda = \Sigma[W(\lambda, T)\{I_{obs}(\lambda) - I_{syn}(\lambda, T)\}]\Delta\lambda$.

The W.R.E. spectroradiometer was used with resolutions of 1.6 and 5.0 nm. It records logarithmically. The photomultiplier dark current is within the span of the amplifier, and any foreground sky, or underlying continuum, can be detected. Also, the amplifier has a frequency response beyond 1 kHz, which makes shot noise in the photomultipliers evident. However, the intensity

and sensitivity *vs.* wavelength calibrations of this instrument are good. When the output is compared with the model, it is difficult to detect differences of less than 100 K because of the photomultiplier shot noise. There is good agreement between the 1.5 and 5.0 nm resolution spectra.

The echelle spectrograph has a resolution of about 0.07 nm, and records photographically, i.e. on a logarithmic scale. Its output is degraded by noise from the microdensitometer because a very narrow slit is needed to resolve the rotational structure (see figure 21). We had hoped to use this instrument to make a detailed comparison of the observed and theoretical intensities of the rotational structure in the bands, but difficulties in obtaining sufficiently accurate calibrations ot sensitivity against wavelength and intensity made this impossible. We were, however, able to detect the effects of Fraunhofer absorption in the excitation process. Overall fits of the model to the data did not enable the temperature to be determined to better than 100 K.

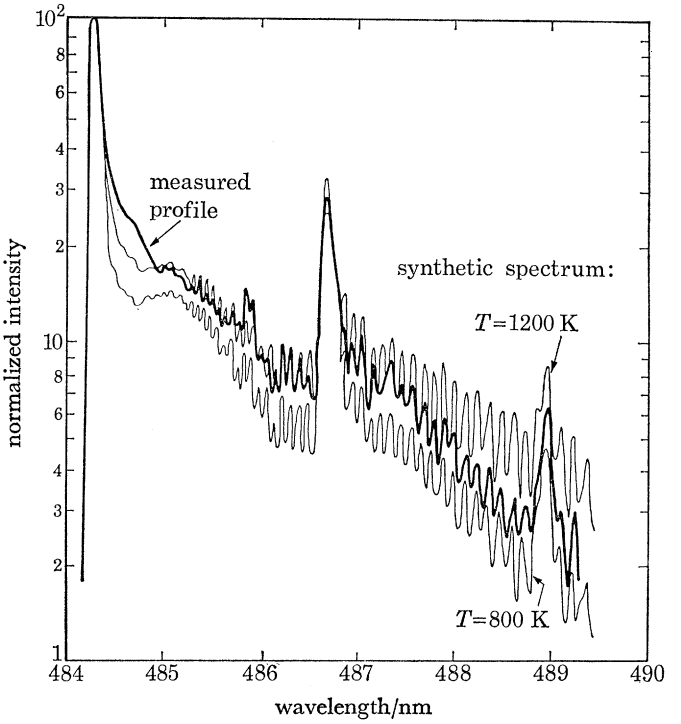

FIGURE 21. AlO $A^2\Sigma$–$X^2\Sigma$, $\Delta v = 0$, sequence from echelle spectrograph.

Figure 21 gives a typical normalized densitometer tracing across an echelle spectrograph record, and the theoretical spectrum for temperatures of 1200 and 800 K. A temperature of 1000 K was found to give the best fit to the data. It has been found easier and more satisfactory to smooth the theoretical curve with the instrument slit function, than to remove this smoothing from the data. The great dispersion of the instrument, which partially resolves the rotational structure, means that the fit of the theoretical curves to the data may be applied to fine detail in the spectrum, which is not possible with the spectroradiometers. This fine detail means, however, that extreme care must be made in modelling the theoretical curve; in particular the Fraunhofer lines of the solar spectrum must be included in detail. The Utrecht Atlas of the solar spectrum (Minnaert, Mulders & Houtgast 1940) was used to do this together with data from Rozenberg (1966). The difference between vacuum and atmosphere wavelength must also be included. On

the benefit side, the fine detail allows the intensity calibration to be checked, by comparing the consistency of an experimentally determined spectrum with the theoretical curves at the temperature which gives the best fit. Since the echelle spectrograph observes the whole spectral range at the same time, no errors are introduced by the instrument tracking on to parts of the cloud which have different intensity during the exposure – sometimes a source of error in the spectroradiometers.

Figures 18 and 19 contain all the measured temperatures. The points at around 100 km on figure 18 were obtained from the shock wave velocity in the trail. All the other points were obtained from the AlO band spectrum. The agreement between the various instruments is good, except that the values obtained from the echelle spectrograph in the evening, with the exception of the highest release, are consistently high. In view of the agreement of the other two sets of results, this is probably due to calibration difficulties experienced during the evening firing.

It will be seen that the values obtained from the clouds at around 240 km are low. At these altitudes the collision frequency may not be high enough to maintain a Maxwellian distribution in the ground electronic state, but there is no indication of this in the observed spectra. Furthermore, Harang (1969) has shown that thermal equilibrium between the AlO molecules and the ambient atmosphere probably exists up to altitudes as great as 300 km. Therefore we believe that the temperature minimum at around 240 km is a real effect. Paetzold (1963) has deduced a similar minimum in the temperature profile at 220 km from his observations of scale heights determined from satellite orbits, and Shchepkin (1969) has reported a possible neutral gas temperature maximum at 200 km from rocket observations. No one has attempted to explain these results. They are most likely produced by a heat source at around 200 km. Because of the high conductivity at these altitudes, the proposed heating could produce a temperature maximum in the profile only if accompanied by considerable horizontal transport. Whether or not horizontal winds at these altitudes could support such a temperature maximum must await their determination on a global scale.

Although the scatter of the data is almost as large as any systematic difference between the morning and evening data, we feel that the higher morning temperature below 170 km and higher evening temperature above 170 km are real.

TABLE 7. DATA APPERTAINING TO THE EXOSPHERIC TEMPERATURE

	morning	evening
mean 10.7 cm flux over 3 solar rotations	142.3	142.3
solar 10.7 cm flux 31 May 1968	146.0	146.0
local mean solar time of firing	05h45	17h55
geomagnetic K_p index 6 h before trial	2	3

We have compared the observations with the *U.S. Standard Atmosphere Supplements* (1966). The method of determining the exospheric temperature is given in detail in the prologue to the tables of the model atmosphere. The relevant information is given in table 7; it is found that the model morning and evening exospheric temperatures are 980 and 1150 K respectively. Below 120 km the model atmosphere does not depend on the exospheric temperature; the atmosphere which corresponds closest to the conditions of our experiment is the model for 30° N January. The model temperature profiles are plotted on figures 18 and 19. It is seen that the agreement with the morning observations is extremely good. The observed evening temperatures, however, do not agree with the model – the observed temperature is consistently 150 to 200 K lower.

Diffusion coefficient

The trail and glow clouds were photographed by the $f/1$, 49.45 cm focal length Baker Nunn camera located at Woomera, and by several $f/1.4$, 85 mm focal length 35 mm cameras. The clouds were also recorded by the scanning photometer described by Johnson & Lloyd (1963). These records complemented one another – the long focal length of the Baker Nunn camera enabled records to be obtained of the trail with high resolution. The sensitivity of the scanning photometer enabled good records to be obtained of the diffuse high-altitude glow clouds. The comparatively large field of view of 23° × 17° of the staggered 35 mm cameras enabled continuous data to be obtained on all the glow clouds for 250 s after release in the case of the TMA trail, and to 500 s after release for the highest glow clouds.

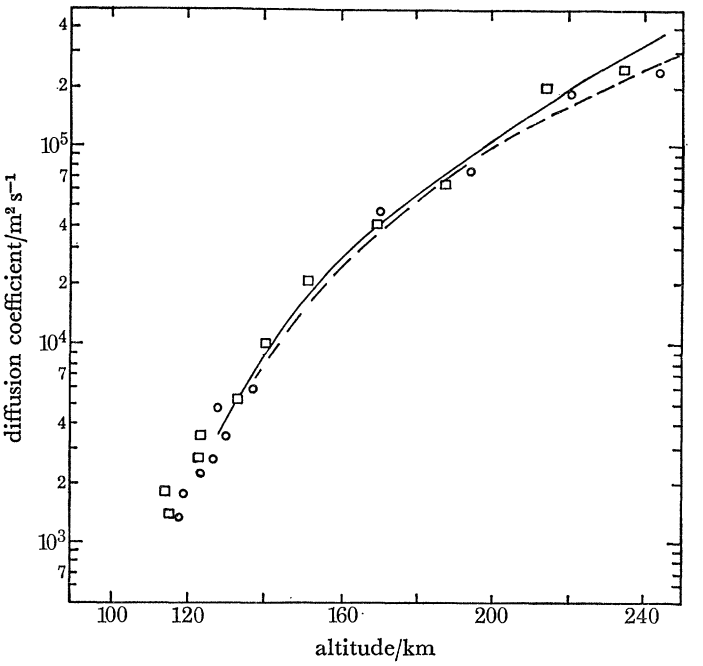

Figure 22. Diffusion coefficient. ○, SL 761 (morning); □, SL 762 (evening).

The photographs of the clouds were analysed by using an Isodensitracer, similar to the one described by Golomb & MacLeod (1966). The diffusion coefficient is determined from these records by plotting the square of the effective radius against time (Lloyd & Sheppard 1966): the equation describing the diffusion of the cloud is

$$\partial n/\partial t = D\nabla n^2 - kn, \tag{7}$$

where n is the number density, and D is the diffusion coefficient, assumed to be independent of concentration. The last term represents loss by chemical reactions; Johnson *et al.* (1967) have shown that above 130 km this linear dependence on n is a good approximation. The solution of equation (7), for a spherical release with an initial Gaussian distribution of effective radius r_0, is

$$n = \frac{n_0 e^{-kt}}{(1+4Dt/r_0^2)^{\frac{3}{2}}} \exp\left[-r^2/(r_0^2+4Dt)\right].$$

Figure 22 shows the results for the diffusion coefficient. Generally, a value for each cloud was obtained from each piece of equipment, and the mean of these has been plotted. Between 140 and

200 km the agreement between the results from the different instruments was within 15 %, and this is the sort of error we expect from these observations. Above 200 km and below 140 km the agreement was not as good. At the low altitudes the observed diffusion coefficient was found to change rapidly with altitude. Rees (1968) has observed similar phenomena from observations of TMA trails released over Pakistan in which the diffusion coefficient actually decreased with an increase of altitude over some part of the range 100 to 110 km.

We found that the diffusion coefficient throughout the altitude region 100 to 130 km was somewhat above the molecular value. This confirms the hypothesis we made earlier that there is always some turbulence in this region, and that the change from globular to laminar at 105 km, observed by Golomb & MacLeod (1966), reflects a change in the scale or type of turbulence, rather than a cessation of turbulence. It is interesting that the observations reported here agree with those made by Lloyd & Sheppard (1966) on grenade glow clouds between 100 and 130 km, but do not agree with the observations of Golomb & MacLeod (1966), who found that the diffusion in the trail was molecular down to 100 km. Zimmerman (1966*c*) had suggested that the difference between Golomb & MacLeod's results and those of Lloyd & Sheppard was that the release of the trail did not produce any turbulence, whereas the explosion of the grenade did. The results reported here show that this is not the case, and that enhanced diffusion can occur even in a smooth trail release.

The variation in the values of diffusion coefficient from different instruments on the same cloud above 200 km is probably due to the presence of barium ions in close proximity to the neutral AlO cloud. The contribution of these ions to the radiance is about 20 %, and is sufficient to produce a detectable non-sphericity; this is caused by the differential drift of the neutral and ionized clouds, since the latter are constrained to diffuse along the Earth's magnetic field lines. The observing instruments were located at different stations, and so their results were affected differently.

Figure 22 shows that there is a diurnal variation in the diffusion coefficient, which is best discussed in terms of density, derived from the diffusion coefficient in the next section.

Density

From the results for temperature and diffusion coefficient the atmospheric density can be determined from the relation

$$\rho = \frac{3}{8D\sigma^2}\left[\frac{kTm\,M_{\mathrm{A}}(M_{\mathrm{A}}+M_{\mathrm{c}})}{2\pi M_{\mathrm{c}}}\right], \tag{8}$$

where D is the diffusion coefficient, k the Boltzmann constant, m the mass of the hydrogen atom, M_{c} the molecular mass of the contaminant, M_{A} the molecular mass of the atmosphere σ, the collision diameter, and ρ the atmospheric density, which is derived from Chapman & Cowling (1952, p. 250). The variation in the collision diameter, σ, with temperature is given by Hirschfelder, Curtiss & Bird (1954) as

$$\sigma^2 = \sigma_0^2\,\Omega(1,1)^*(T^*),$$

where σ_0 is independent of temperature, but depends on the molecular species, and $\Omega(1,1)^*(T^*)$ is a tabulated function of $T^* = T(\Sigma/k)^{-1}$, and also depends on the molecular species. Hirschfelder, Curtiss & Bird (1954) quote Σ/k for many gases; plotting these as a function of molecular weight shows that both these quantities increase slowly, and more or less linearly, with molecular weight. The average trend can be represented by $\sigma_0 = 3.63 \times 10^{-10}$ m and $\Sigma/k = 80$ K at $M = 28$, and

$\sigma_0 = 3.90 \times 10^{-10}$ m, $\Sigma/k = 150$ K at $M = 43$. For the interdiffusion of two gases, the mean value to be used is

$$\sigma = \tfrac{1}{2}(\sigma_1 + \sigma_2) \quad \text{and} \quad \Sigma = (\Sigma_1 \Sigma_2)^{\frac{1}{2}}.$$

The relatively large uncertainty in the value of Σ/k is not serious, because $\Omega(1, 1)^*(T^*)$ is a very slowly varying function of T^*. The probable error in σ is estimated to be about 4 %.

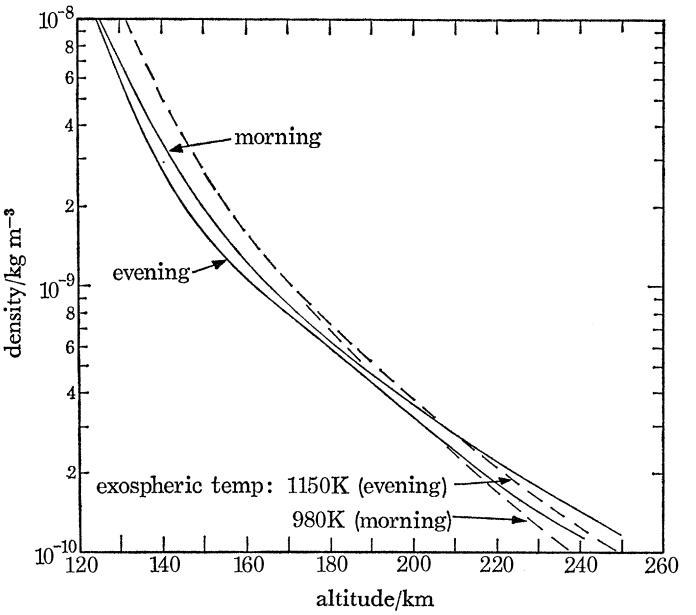

FIGURE 23. Density profile. *U.S. Standard Atmosphere Supplements* (1966) (– – –).

Figure 23 shows the density profiles for the morning and evening firings calculated from the observed temperature and diffusion data by using equation (8). The profiles from the *U.S. Standard Atmosphere Supplements* (1966) for exospheric temperatures of 980 and 1150 K are also plotted. The observations are less than the model below 160 km, but agree well with the model above 180 km. Furthermore, the observed diurnal behaviour is quite different from the prediction of the model – we observe the morning density above 170 km to be greater than the evening density. Since this is such a fundamental difference, it prompts one to suspect the original diffusion data. However, we feel that the difference shown in the morning and evening values of the diffusion coefficient is significant.

Satellite results unequivocably show that, at high altitudes, the evening density exceeds the morning density; from our results it seems that perhaps this happened above 250 km, but not around 160 km as the model atmospheres predict. As pointed out in the text of the *U.S. Standard Atmosphere Supplements* (1966), the predicted 160 km isopycnic is not real, but results from the choice of 120 km as an isopycnic for the lower boundary of the model. However, the density at a given altitude *is* intimately related to that at lower altitudes, and to the temperature profile. The reason for the increased density during the day at high altitudes is that the underlying layers are heated and their density falls. To preserve the hydrostatic balance, the higher altitude density increases. Since the density decreases rapidly with altitude, the fractional change in density at high altitudes is much greater than the fractional change at low altitudes. This makes it impossible to determine whether our reversed temporal density behaviour at 240 km has associated departures at lower altitudes. We are left to speculate on whether there may be some connexion between what appears

to be a temperature minimum around 250 km and the observed diurnal density variation. If in fact there were additional sources of heating at 200 km (regarding the temperature at 200 km as a peak, rather than the temperature at 250 km as a trough) we would expect them to produce corresponding changes in density. Unfortunately our limited data preclude a qualitative examination of such effects. Suffice here to say that they suggest processes occurring in the region 200 to 250 km which have not hitherto been considered, and which would bear further investigation.

A comparison of the observed and model profiles shows that the observations show a scale height which is greater than expected from the model: 89 km at 200 km altitude compared with 73 km. Golomb *et al.* (1968) have observed a similar departure from the model atmosphere.

Summary

The analysis of the contaminant releases, made on the morning and evening of 31 May 1968, has shown the following characteristics in the diurnal behaviour of the atmosphere in the altitude region 80 to 250 km:

(1) The neutral wind structure function showed that the atmosphere was more turbulent in the evening; this was confirmed, not only by measurements of the turbulent intensity, but also by the fact that the turbopause was higher in the evening. The turbulent intensity did not correlate with the wind shears, which were higher in the morning, suggesting that, at least in this case, the turbulent intensity was determined by the temperature profile rather than by the wind shear.

(2) The change in the trail from dehiscent to laminar behaviour, which has always been associated with the turbopause, was seen to occur at the altitude where the time constant of the Kolmogoroff microscale increased extremely rapidly with altitude. Coupled with this was the observation that the onset of turbulence in the trail was determined by this same time constant, and not by the condition that the trail size had reached the size of the Kolmogoroff microscale.

(3) The wind velocity above 200 km showed a diurnal pattern and agreed with the finding by King-Hele that the eastward winds are strongest in the evening. Meridional components were, however, of the same magnitude as the zonal winds.

(4) A study of the comparative lifetime of the chemiluminescent glow clouds, when compared with previous releases above Woomera, showed a strong seasonal variation. This indicates a large seasonal dependence in the chemical species associated with the chemiluminescence, most probably atomic oxygen.

(5) The morning temperature profile followed the *U.S. Standard Atmosphere Supplements* (1966) extremely closely, but the evening temperature profile was lower than the model by about 150 to 200 K.

(6) There was some evidence for a temperature inversion above 200 km, both in the morning and in the evening.

(7) The observed densities were lower than the *U.S. Standard Atmosphere Supplements* (1966) for the appropriate solar conditions, below about 200 km, and higher than the model above 200 km.

(8) The diurnal behaviour showed the density to be greater in the morning than in the evening. This is quite different from the predictions of the model atmosphere, and it is tentatively suggested that this may be related to the temperature inversion above 200 km.

This project was supported by the British Science Research Council and Ministry of Technology, and the Australian Department of Supply; the payloads and rockets being prepared by

PHILOSOPHICAL TRANSACTIONS OF THE ROYAL SOCIETY A MATHEMATICAL, PHYSICAL & ENGINEERING SCIENCES

the Space Science and Atmospheric Structure Group, University College London, and the Aerodynamics Division, Weapons Research Establishment, Salisbury, South Australia, and fired at the Woomera Rocket Range. Range support was given jointly by B.D.R.S.S. and W.R.E. Woomera authorities. Support for data analysis at U.C.L., and for optical ground equipment, has been provided by the Air Force Cambridge Research Laboratories through the European Office of Aerospace Research under Contract AF 61(052)-781.

We should like to thank the Mathematics Services Group, and Aerodynamics Division Computing Section, W.R.E., and Space Science and Atmospheric Structure Group, U.C.L., for their considerable assistance with the data analysis of the project. The staff of Baker Nunn camera at Deep Space Station 41, Woomera, kindly provided photographs that they had taken of the releases.

References

Armstrong, E. B. 1963 *Planet. Space Sci.* **11**, 733.
Authier, B., Blamont, J. E. & Carpentier, F. 1962 *C. r. hebd. Séanc. Acad. Sci., Paris*, **255**, 1974.
Batchelor, G. K. 1953 *The theory of homogeneous turbulence*. Cambridge University Press.
Becart, M. & Declerck, F. 1960 *C. r. hebd. Séanc. Acad. Sci. Paris*, **251**, 2153.
Blamont, J. E. 1961 *C. r. hebd. Séanc. Acad. Sci. Paris*, **249**, 1248.
Blamont, J. E. 1963 *Planet. Space Sci.* **10**, 89.
Blamont, J. E. & Barat, J. 1967*a* *Annls Géophys.* **23**, 173.
Blamont, J. E. & Barat, J. 1967*b* *Aurorae and airglow* (ed. B. M. McCormac), p. 159. New York: Reinhold Publ. Co.
Blamont, J. E. & Barat, J. 1968 *Annls Géophys.* **24**, 375.
Blamont, J. E. & De Jager, C. 1961 *Annls Géophys.* **17**, 134.
Blamont, J. E. & Lory, M. L. 1964 *C.N.R.S. Service d'Aeronomie Rep.* no. 15.
Bolgiano, R. 1959 *J. geophys. Res.* **64**, 2226.
Bolgiano, R. 1962 *J. geophys. Res.* **67**, 3015.
Booker, H. B. & Cohen, R. 1956 *J. geophys. Res.* **61**, 707.
Brandy, J. H. 1964 *Can. J. Phys.* **42**, 1793.
Brandy, J. H. 1965 *Can. J. Phys.* **43**, 1697.
Challinor, R. A. 1968 *Planet. Space Sci.* **16**, 557.
Challinor, R. A. 1969 *Planet. Space Sci.* **17**, 1097. (See also correction in *Planet. Space Sci.* **18**, 1485 (1970).)
Chapman, S. & Cowling, T. G. 1952 *The mathematical theory of non-uniform gases* (2nd ed.). Cambridge University Press.
Colegrove, F. D., Johnson, F. S. & Hanson, W. B. 1966 *J. geophys. Res.* **71**, 2227.
Cook, G. E. & Scott, D. W. 1967 *Planet. Space Sci.* **15**, 1933.
Doyle, E. M. 1969 Ph.D. Thesis, University of Adelaide.
Elford, W. G. & Doyle, E. M. 1972 Wind measurements near 90 km (1966–68). (To be published.)
Elford, W. G. & Roper, R. G. 1967 *Space Research VII* (ed. R. L. Smith-Rose), p. 42. Amsterdam: North Holland Publ. Co.
Föppl, H., Haerendel, G., Haser, L., Loidl, J., Lütjens, P., Lüst, R., Melzner, F., Meyer, B., Neuss, H. & Rieger, E. 1967 *Planet. Space Sci.* **15**, 357.
Golomb, D., Delgreco, F. P., Harang, O., Johnson, R. H. & MacLeod, M. A. 1968 *Space Research VIII* (ed. A. P. Mitra, L. G. Jacchia & W. S. Newman), p. 705. Amsterdam: North Holland Publ. Co.
Golomb, D. & MacLeod, M. A. 1966 *J. geophys. Res.* **71**, 2299.
Goodlet, V. W. & Innes, R. R. 1959 *Nature, Lond.* **183**, 243.
Greenhow, J. S. & Neufeld, E. L. 1959 *J. geophys. Res.* **64**, 2129.
Groves, G. V. 1960 *Nature, Lond.* **187**, 1001.
Groves, G. V. 1963 *J. geophys. Res.* **68**, 3033.
Harang, O. 1967 *Phys. Norvegia* **2**, 71.
Harang, O. 1969 *Tromsö Auroral Observatory Sci. Rep.* no. 1.
Harris, I. & Priester, W. 1962 *J. atmos. Sci.* **19**, 286; *J. geophys. Res.* **67**, 4584.
Hines, C. O. 1960 *Can. J. Phys.* **38**, 1441.
Hines, C. O. 1965 *J. geophys. Res.* **70**, 177.
Hines, C. O. 1968 *Monogr. Am. Met. Soc.* **9**, 114.
Hirschfelder, J. O., Curtiss, C. F. & Bird, R. B. 1954 *Molecular theory of gases and liquids*. New York: Wiley.
Hodges, R. R. 1967 *J. geophys. Res.* **72**, 3455.

PHILOSOPHICAL TRANSACTIONS OF THE ROYAL SOCIETY A MATHEMATICAL, PHYSICAL & ENGINEERING SCIENCES

Hooke, W. H. 1969 *J. geophys. Res.* **74**, 1870.
Jacchia, L. G. 1965 *Smithson. Contr. Astrophys.* **8**, 215.
Johnson, E. R. 1965 *J. geophys. Res.* **70**, 1275.
Johnson, E. R. 1968 *W.R.E. Tech. Note HSA* 136.
Johnson, E. R. & Lloyd, K. H. 1963 *Aust. J. Phys.* **16**, 490.
Johnson, E. R., Lloyd, K. H., Low, C. H. & Sheppard, L. M. 1967 *Aust. J. Phys.* **20**, 683.
Johnson, E. R. & Low, C. H. 1967 *Aust. J. Phys.* **20**, 5.
Johnson, F. S. 1967 *Space Research VII* (ed. R. L. Smith-Rose), p. 262. Amsterdam: North Holland Publ. Co.
Justus, C. G. 1966 *J. geophys. Res.* **71**, 3767.
Justus, C. G. 1967*a* *J. geophys. Res.* **72**, 1933.
Justus, C. G. 1967*b* *J. geophys. Res.* **72**, 1035.
Justus, C. G. & Roper, R. G. 1968 *Monogr. Am. Met. Soc.* **9**, 122.
King-Hele, D. G. & Scott, D. W. 1967 *Planet. Space Sci.* **15**, 1913.
King-Hele, D. G. 1970 *Nature, Lond.* **226**, 439.
Kochanski, A. 1963 *J. geophys. Res.* **68**, 213.
Kochanski, A. 1964 *J. geophys. Res.* **69**, 3651.
Kochanski, A. 1965 *World Meteorol. Tech. Note* **70**, p. 140.
Kolmogoroff, A. N. 1941 *Dokl. Akad. Nauk. SSSR Moscow* **30**, 301.
Lagerquist, A., Nilsson, N. E. L. & Barrow, R. F. 1957 *Ark. Fys.* **2** (25), 543.
Lindzen, R. S. 1966 *Mon. Weather Rev. U.S. Dep. Agric.* **94**, 298.
Lindzen, R. S. 1968 *Monogr. Am. Met. Soc.* **9**, 37.
Lloyd, K. H. & Sheppard, L. M. 1966 *Aust. J. Phys.* **19**, 323.
Lloyd, K. H., Low, C. H., McAvaney, B. J., Rees, D. & Roper, R. G. 1972 *Planet. Space Sci.* (In the press.)
Low, C. H. 1967 *Planet. Space Sci.* **15**, 199.
Lumley, J. L. 1964 *J. Atmos. Sci.* **21**, 99.
Manring, E., Bedinger, J. & Knaflich, H. 1961 *Space Research II* (ed. H. G. Van de Hulst, C. de Jager & A. F. Moore), p. 1107. Amsterdam: North Holland Publ. Co.
Meadows, E. B. & Townsend, J. W. 1958 *Annls Géophys.* **14**, 80.
Meadows, E. B. & Townsend, J. W. 1960 *Space Research I* (ed. H. Kallman-Bijl), p. 175. Amsterdam: North Holland Publ. Co.
Minnaert, M., Mulders, M. F. W. & Houtgast, J. 1940 *Photometric atlas of the solar spectrum* ('*Utrecht Atlas*'). Amsterdam: Kampert and Helm.
Müller, H. G. 1968 *Planet. Space Sci.* **16**, 61.
Paetzold, H. K. 1963 *Space Research III* (ed. W. Priester), p. 28. Amsterdam: North Holland Publ. Co.
Rees, D. 1967 Ph.D. Thesis, London University.
Rees, D. 1968 *Space Research VIII* (ed. A. P. Mitra, L. G. Jacchia & W. S. Newman), p. 909. Amsterdam: North Holland Publ. Co.
Rees, D. 1969 *J. Br. interplanet. Soc.* **22**, 275.
Rees, D. 1971 *Planet. Space Sci.* **19**, 233.
Rees, D. 1972 *Phil. Trans. R. Soc. Lond.* A **271**, 563.
Rofe, B. 1961 *W.R.E. Tech. Memo. SAD* 125.
Roper, R. G. 1966*a* *J. geophys. Res.* **71**, 5785.
Roper, R. G. 1966*b* *J. geophys. Res.* **71**, 4427.
Roper, R. G. & Low, C. H. 1969 *W.R.E. Tech. Note HSA* 161.
Roper, R. G. & Elford, W. G. 1963 *Nature, Lond.* **197**, 963.
Rosenberg, N. W. 1964 *J. geophys. Res.* **69**, 2323.
Rosenberg, N. W. 1968*a* *J. atmos. terr. Phys.* **30**, 907.
Rosenberg, N. W. 1968*b* *J. geophys. Res.* **73**, 4965.
Rosenberg, N. W., Golomb, D. & Allen, E. F. 1963 *J. geophys. Res.* **68**, 5895.
Rosenberg, N. W. & Justus, C. G. 1966 *Radio Sci.* **1** (new series), 149.
Rozenberg, G. V. 1966 *Twilight: a study in atmospheric optics*. New York: Plenum Press.
Shchepkin, L. A. 1969 *Geomagn. Aeron.* **9**, 161.
Spizzichino, A. 1969 *Annls. Géophys.* **25**, 693.
Stoffregen, W. 1968 *Ann. Rep. Uppsala Ionsp. Inst.* 1967–1968.
Sullivan, K. M. & Roberts, M. G. 1968 *Nature, Lond.* **220**, 361.
U.S. Standard Atmosphere Supplements 1966 Washington: U.S. Govt. Printing Office.
Wand, R. H. & Perkins, F. W. 1968 *J. geophys. Res.* **73**, 6370.
Zimmerman, S. P. 1966*a* *Proceedings of the conference on ground-based radio-wave propagation studies of the lower ionosphere* (ed. Belrose), p. 97. Ottawa: Defense Res. Telecoms. Estab.
Zimmerman, S. P. 1966*b* *J. geophys. Res.* **71**, 2439. (Note also correction in *J. geophys. Res.* **72**, 5153 (1967).)
Zimmerman, S. P. 1966*c* *Space Research VI* (ed. R. L. Smith-Rose), p. 425. Washington: Spartan Books.

PHILOSOPHICAL TRANSACTIONS OF THE ROYAL SOCIETY A MATHEMATICAL, PHYSICAL & ENGINEERING SCIENCES

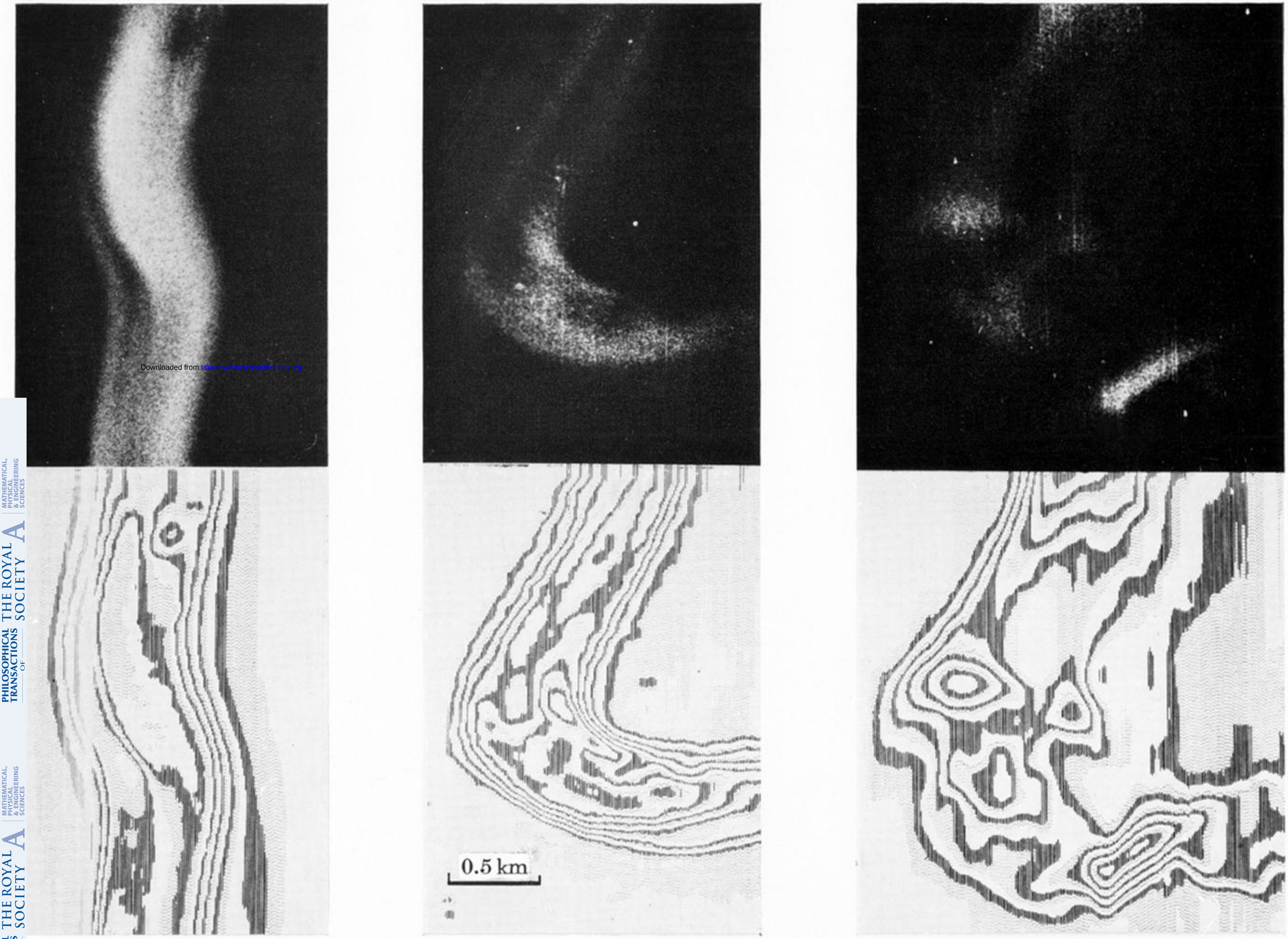

$t = +5$ $+30$ $+50$ s after release

FIGURE 4. Montage of portion of the morning trail. The kink is at an altitude of 102.7 km. Note that the trail is laminar at $+30$ s, and that the trail diameter at this time is greater than the scale of the eddies at $+50$ s.

PHILOSOPHICAL TRANSACTIONS OF THE ROYAL SOCIETY A MATHEMATICAL, PHYSICAL & ENGINEERING SCIENCES

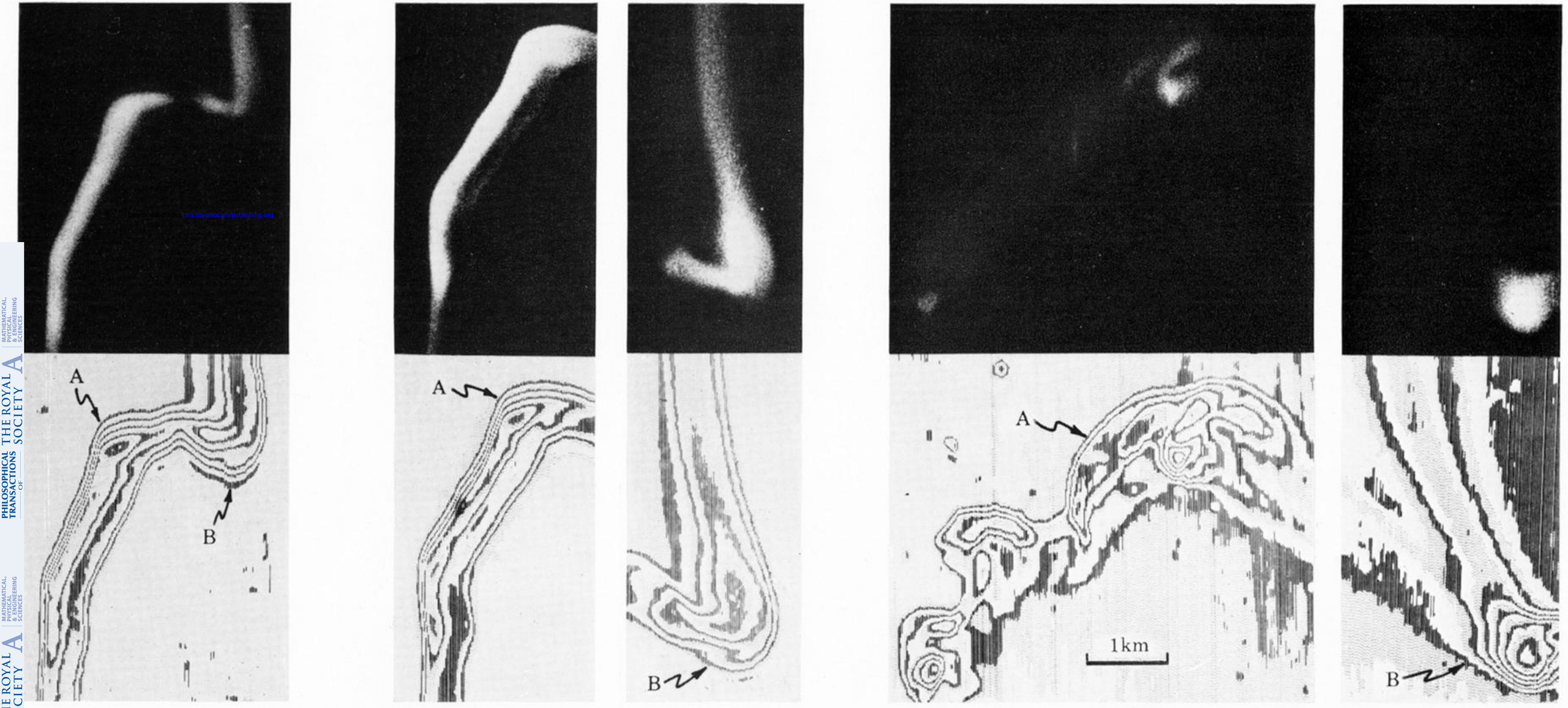

FIGURE 5. Montage of portions of the evening trail. Points A and B are at 106 and 108 km altitude respectively. Note the transition from laminar to turbulent structure at A between +23 and +61 s. This has not occurred at B.

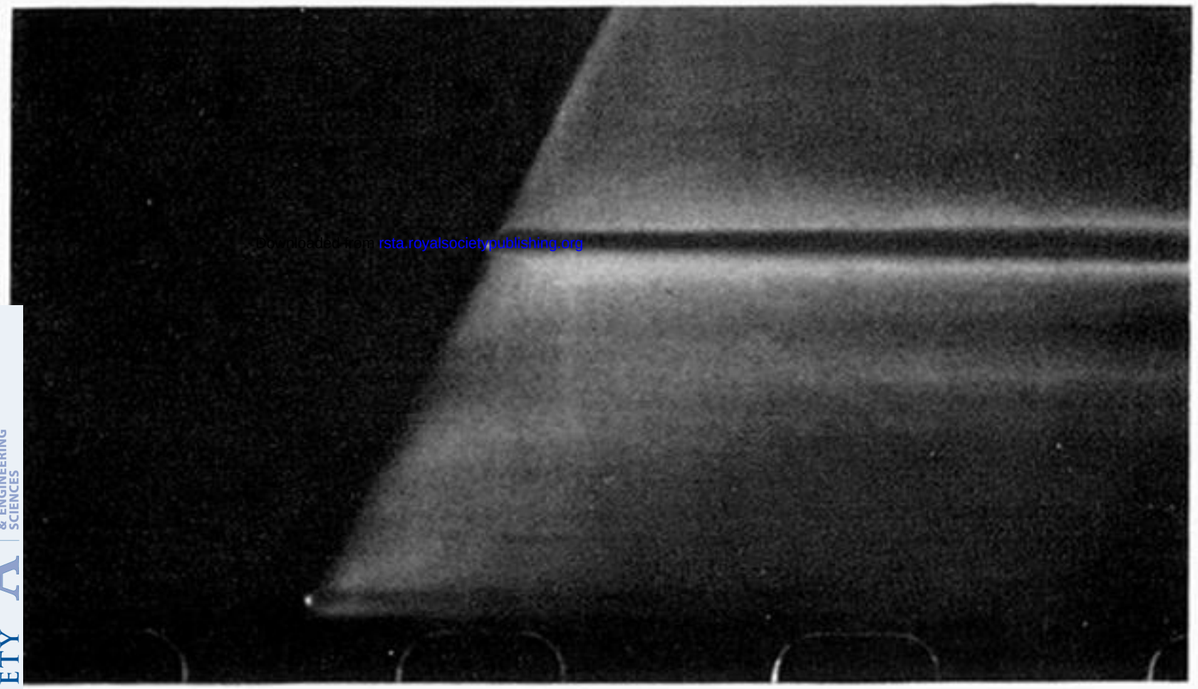

C

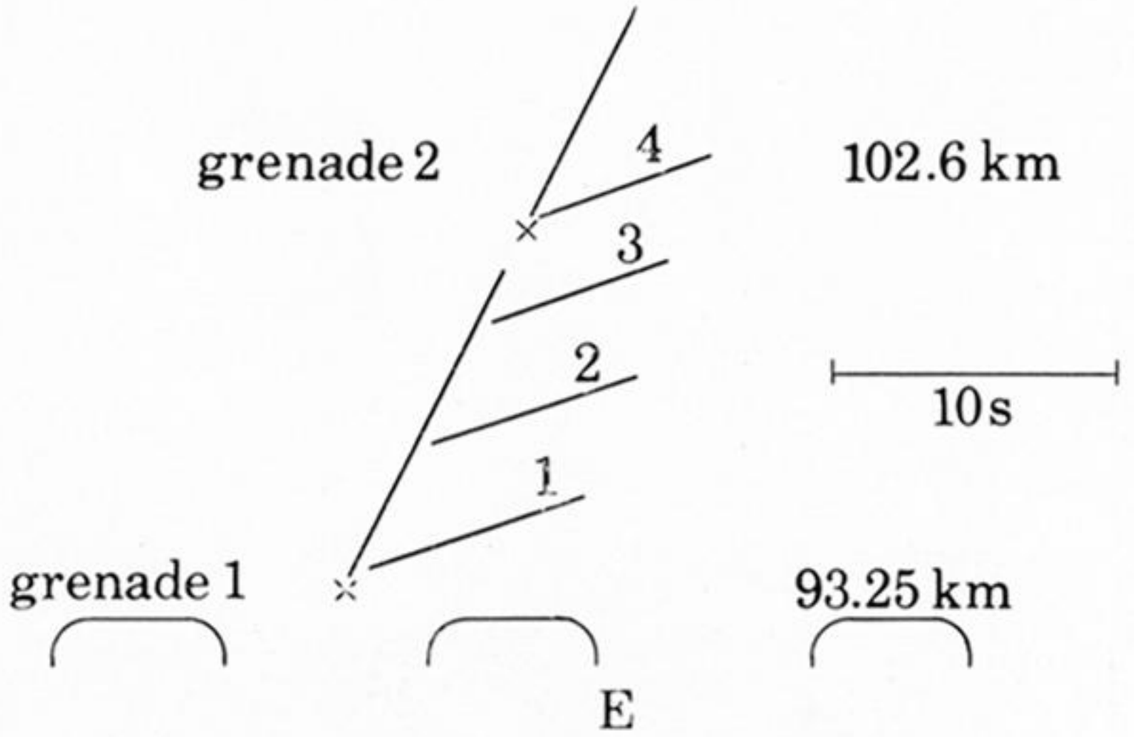

E

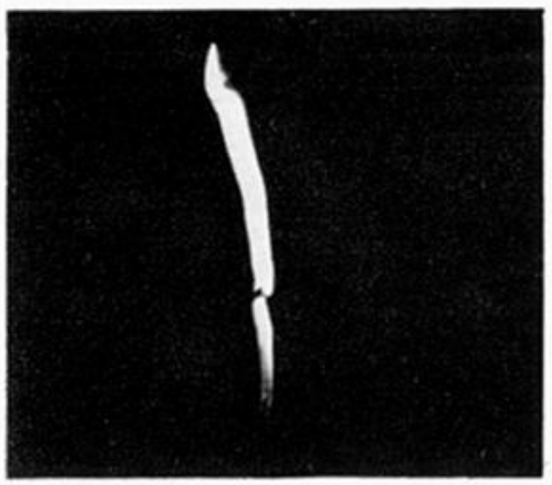

D

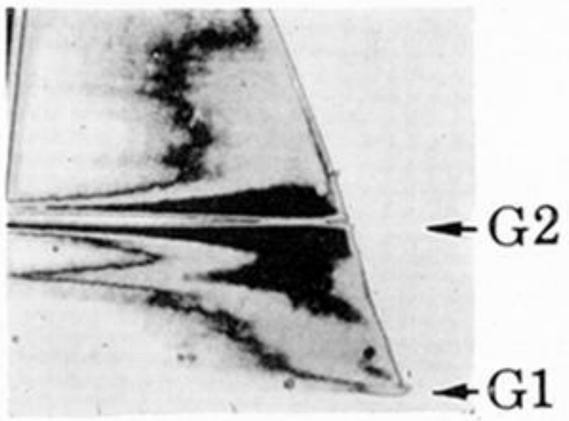

A

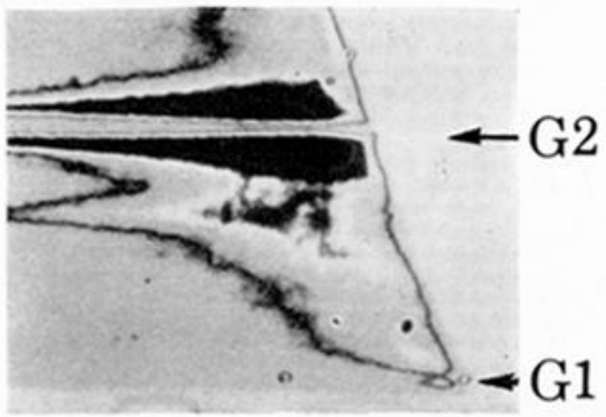

B

FIGURE 12. Montage of streak camera analysis on morning trail. A, Polaroid print of television screen, shock waves as light features. B, Polaroid print of television screen, shock waves as dark features. C, Print of streak camera photograph. D, Baker Nunn photograph at 78 s after launch. E, Identification of measured features: 1, upward shock wave envelope of G 1; 2, ground shock wave 3 (40 kg); 3, ground shock wave 2 (20 kg); 4, upward shock wave envelope of G 2.

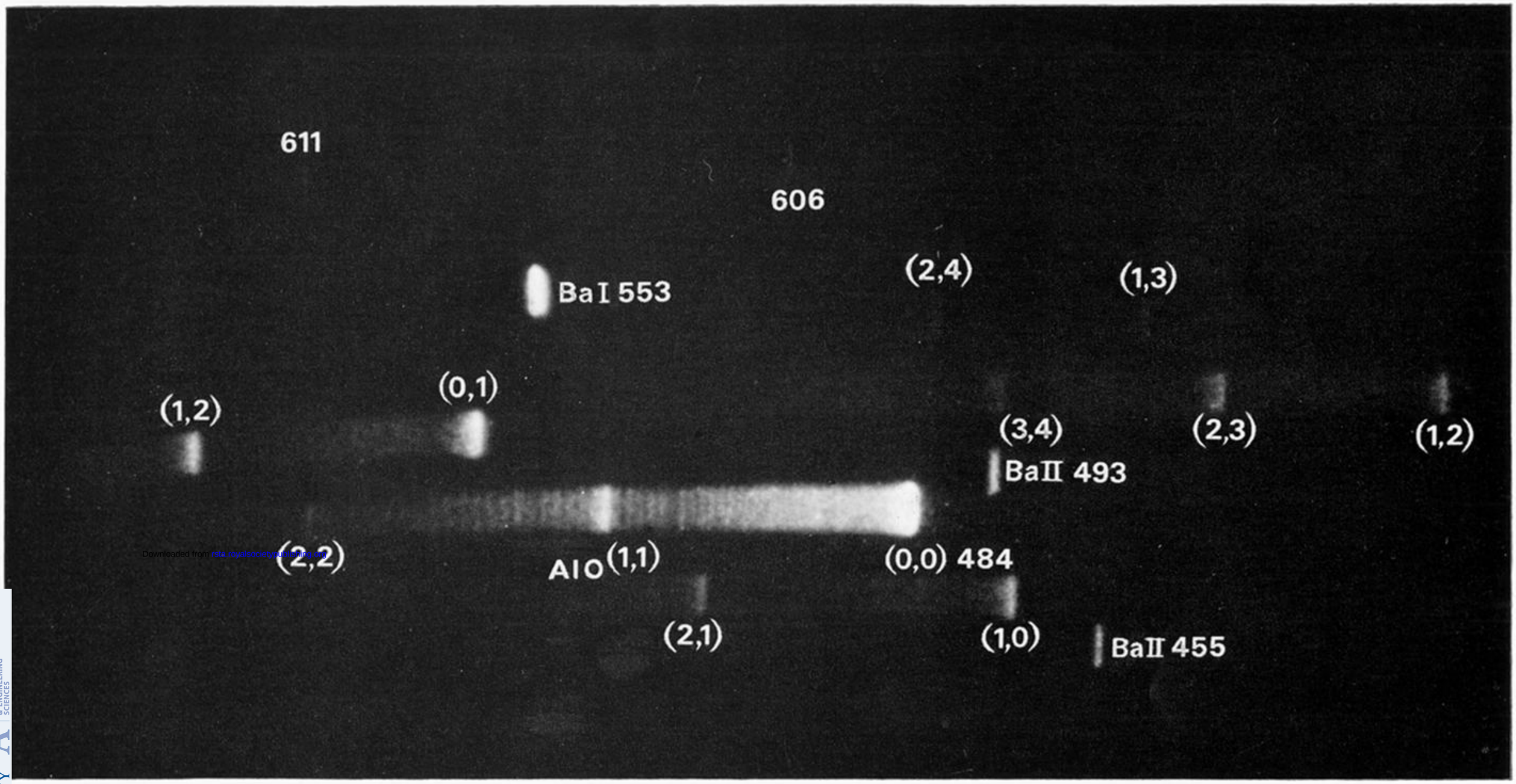

FIGURE 14. Echelle plate from the glow cloud at 187 km on the evening firing. The features observed from all the glow clouds on trials SL 761 and SL 762 are listed.

barium lines		AlO					
Ba I	Ba II	order	λ/nm	band	order	λ/nm	band
553.5	455.4	46	536	(1, 3)	48	508	(0, 1)
582.6	493.4	46	538	(2, 4)	48	510	(1, 2)
597.7	614.2	46	539	(3, 5)	50	484	(0, 0)
599.7	649.2	47	510	(1, 2)	50	487	(1, 1)
606.3		47	512	(2, 3)	50	489	(2, 2)
611.0		47	514	(3, 4)	52	465	(1, 0)
634.2		47	516	(4, 5)	52	467	(2, 1)
649.9							
652.7							
667.5							
669.3							
706.0							

PHILOSOPHICAL TRANSACTIONS OF THE ROYAL SOCIETY A MATHEMATICAL, PHYSICAL & ENGINEERING SCIENCES